Chapter 8. Flight Test of Clock Aided Positioning

8.1 Background

A flight test was conducted using the Ohio University Flight Reference/Autoland System during which Ashtech Z-12 receivers were augmented by external rubidium clocks. The purpose was to evaluate the accuracy of clock-aided solutions as compared to other DGPS position solutions, particularly in the vertical direction, and to demonstrate three-satellite navigation using stable clocks. This study focuses on approach and landing because vertical accuracy is most critical during this phase of flight. The FAA sponsored the flight tests as part of a program to demonstrate the potential of differential GPS as a landing system under conditions of poor visibility. A description of the different solutions is followed by the flight test results and analysis.

8.2 Differential GPS Solutions

In this section, the differential GPS solutions used in this chapter to analyze the flight data collected at Atlantic City are presented. These solutions rely heavily on the concepts of single and double differencing, which were covered in Section 3.4. Most of the solutions presented are based on code-phase, or pseudorange measurements. However, carrier phase measurements were used in the PNAV truth reference as well as in one of the clock-aided solutions. Except for the PNAV solution, only the L_1 (1575.42 MHz) signal was used during

analysis of the flight data. Thus, a basis of comparison is presented for the clock-aided GPS solutions and the unaided GPS solutions.

8.2.1 Solutions without Clock Aiding

8.2.1.1 Ashtech PNAV Solution

The PNAV software is part of the Ashtech PRISM package and can be used to calculate position using code and carrier phase from data collected from the ground and airborne Z-12 receivers. Both L1 (1575.42 MHz) and L2 (1227.6 MHz) carrier phase measurements are used by PNAV to calculate accurate position. By using both frequencies, a widelane observable can be formed which eases the task of ambiguity resolution. The widelane comes from differencing L1 and L2 measurements to yield an observable with an effective wavelength of about 86 cm (347.82 MHz). The PNAV software can be set for forward processing, backward processing, or both. The selection dictates the ambiguity resolution process. During this analysis, forward processing was used. As a result, the first minute of data from the flight test has not been used to allow the PNAV solution to settle on the correct set of ambiguities before relying on the PNAV solution as a truth reference.

Recall from Eq. 3.13 that a carrier phase measurement, or integrated Doppler, includes an unknown integer number of wavelengths. When the double difference is formed using two receivers and two satellites, a residual integer ambiguity remains (see Eq. 3.16). The widelane technique reduces the number of possible ambiguity sets in a given search volume because the

L_1 - L_2 wavelength is 86 cm. Although the phase noise is increased, the search algorithm for the correct set of ambiguities is more robust. Accuracies of about a quarter wavelength are typical with ambiguity-resolved solutions [Diggle, 1994], so using the widelane should yield a position error of 20 cm or less.

The PNAV software includes several options which can be set before processing the data. Instructions can be given to eliminate a particular satellite or satellites from consideration as the reference satellite. Typically, the highest elevation satellite is used as the reference. Another option is to eliminate a satellite or satellites from the position solution altogether. The output for aircraft position can be expressed as an offset from the ground station in the Earth-Centered Earth-Fixed (ECEF) frame, or in Easting, Northing, and Upping. There is a subtle difference between East, North, Up position and Easting, Northing, and Upping. The latter accounts for Earth curvature and is not used here. Rather, the baseline in ECEF coordinates is used.

A tropospheric model was used but the ionospheric model was turned off. Note that for short baselines, the ionospheric errors approximately cancel due to the high correlation of this error between users that are in close proximity. Another specification can be made for the type of platform on which the roving receiver is located. The selections include static, walking, automobile, and aircraft. The choice is used by PNAV to choose an appropriate set of Kalman filter parameters. Finally, accurate ground station coordinates must be entered for PNAV to produce an accurate solution for aircraft position.

8.2.1.2 Code Phase Single Difference Solution

The single difference is formed by differencing the ground and air pseudorange measurements made to the same satellite. Thus, a combined clock bias term exists:

$$SD_{code} = \Delta code_{rec} + \Delta S_{code} + c\,\Delta t_B \tag{8.1}$$

where: SD_{code} is the code phase single difference (meters)
$\Delta code_{rec}$ represents the difference in the true ranges from the satellite to each receiver (meters)
ΔS_{code} is a combined noise term (meters)
$c\Delta t_B$ is the bias between the ground and air clocks (meters)

Note the absence of an ambiguity term which appears in the carrier phase single difference (Eq. 3.14). Thus, four single differences can be used to unambiguously calculate the baseline, but another state is added to estimate $c\Delta t_B$:

$$\begin{pmatrix} SD^1 \\ SD^2 \\ SD^3 \\ SD^4 \end{pmatrix} = \begin{bmatrix} e_x^1 & e_y^1 & e_z^1 & 1 \\ e_x^2 & e_y^2 & e_z^2 & 1 \\ e_x^3 & e_y^3 & e_z^3 & 1 \\ e_x^4 & e_y^4 & e_z^4 & 1 \end{bmatrix} \begin{pmatrix} bl_x \\ bl_y \\ bl_z \\ c\Delta t_B \end{pmatrix} \tag{8.2}$$

which can be written as:

$$\underline{\boldsymbol{SD}} = H\underline{\boldsymbol{bl}}_c \tag{8.3}$$

where: **SD** is a vector of code phase single difference measurements
H is the geometry matrix with direction cosines to the satellites from the estimated baseline midpoint plus a column of ones for the clock
$\underline{\boldsymbol{bl}}_c$ is the baseline vector plus a clock bias estimate

Because $\underline{\boldsymbol{bl}}_c$ is used extensively later in this chapter, the reader should note that it contains $c\Delta t_B$. The estimate of $c\Delta t_B$ is a noisy approximation of the bias between ground and airborne receiver clocks. If the clock is used as a measurement during periods of high VDOP, $c\Delta t_B$ can be fixed to the last calculated estimate [Lee, 1993] or predicted based on a clock model [Misra, May 1994] using prior data. This is discussed in more detail in Section 8.2.2.

A correction to the single differences is needed which is derived from the fact that the receivers make simultaneous measurements. The satellite time of transmission is different for the ground and airborne receivers, so the satellite position is different at the time of transmission for the airborne (TOT_{air}) and ground (TOT_{gnd}) receivers. Thus, a correction is applied to each single difference:

$$t_{cor} = c(\Delta t_{SVgnd} - \Delta t_{SVair}) + R_{gnd} - R_{air} \tag{8.4}$$

where: t_{cor} is the correction made to the single difference (m)
Δt_{SVgnd} is the satellite clock correction as applied by the ground station (s)
Δt_{SVair} is the satellite clock correction as applied by the air receiver (s)
R_{gnd} is the range from the ground station to the satellite at TOT_{gnd} (m)
R_{air} is the range from the ground station to the satellite at TOT_{air} (m)

The satellite clock correction (Δt_{SV}) is described in Appendix A. R_{gnd} and R_{air} are further corrected for Earth rotation during the signal transmission time, which is called the Sagnac effect

[Ashby & Spilker, 1996]. After all of the corrections have been made to the single differences, the least squares solution of Eq. 8.3 yields an estimate of the baseline and $c\Delta t_B$.

8.2.1.3 Code Phase Double Difference Solution

The code phase double difference solution also uses unambiguous pseudorange measurements to determine the baseline between two receivers, but here the clock bias term drops out. A code phase double difference is calculated following a development similar to the carrier phase double difference of Eq. 3.16. The satellite and receiver clock biases are removed:

$$DD_{code} = \Delta code_{rec}^{12} + \Delta S_{code}^{12} \tag{8.5}$$

where: DD_{code} is the code phase (pseudorange) double difference (m)

$\Delta code_{rec}^{12}$ is the true double difference (m)

ΔS_{code}^{12} is a combined noise term (m)

Although the pseudorange measurements are unambiguous, they are more noisy than carrier phase measurements. Thus, a pure code phase DD solution requires no ambiguity resolution, but is less accurate than an ambiguity-resolved carrier phase DD solution. The code phase solution is given by:

$$\begin{pmatrix} DD_{code}^{12} \\ DD_{code}^{13} \\ DD_{code}^{14} \end{pmatrix} = \begin{bmatrix} e_x^{12} & e_y^{12} & e_z^{12} \\ e_x^{13} & e_y^{13} & e_z^{13} \\ e_x^{14} & e_y^{14} & e_z^{14} \end{bmatrix} \begin{pmatrix} bl_x \\ bl_y \\ bl_z \end{pmatrix} \tag{8.6}$$

which can be written as:

$$\underline{\mathbf{DD}} = H_{diff}\,\underline{\mathbf{bl}} \tag{8.7}$$

where: **DD** is a vector of code phase double differences
H_{diff} is a matrix of differenced direction cosine vectors between the two satellites used where 1 denotes the reference satellite in Eq. 8.6
bl is the baseline between the rover and the ground station

The solution requires at least three double differences (four satellites) and although not implemented here, could be enhanced by incorporating carrier phase measurements. One implementation is a complementary Kalman filter which can be used to couple the unambiguous code phase measurements and the less noisy carrier phase measurements [van Graas & Braasch, 1991-92]. The resulting observables are called smoothed-code double differences, which can be used to solve for the baseline between the two receivers with an accuracy of 1-2 meters [Diggle, 1994]. This float DD solution could be used to help define a search space for an ambiguity resolution algorithm, if desired.

8.2.2 Clock Aided Differential GPS Solutions

Here we modify the code phase single difference solution of 8.2.1.2 to incorporate an estimate of $c\Delta t_B$ which, if accurate, results in the VDOP improvement discussed in Chapter 4. Actually, we attempt to model a combination of clock and hardware drifts. Two methods of estimating the clock and hardware are discussed. One is a standard estimate based on observing $c\Delta t_B$ (which includes hardware variations) over time and fitting a second order polynomial

through the data. The other method uses carrier phase measurements to improve the clock polynomial, taking advantage of the less noisy carrier phase measurements. These techniques will be illustrated in more detail in Sec. 8.3 using data from the Atlantic City flight test.

8.2.2.1 Code Phase Single Difference Solution Using Standard Clock Aiding

The clock state can be modeled by observing $c\Delta t_B$ over some period of time and fitting a second order curve through it in a least squares sense. Note that the clocks and associated hardware must be stable enough to be accurately modeled by a second order curve [Misra, 1995]. Thus, estimates can be based on the following equation [Misra, May 1994]:

$$c\Delta\hat{t}_B(t) = c[k_0 + k_1(t-t_0) + k_2(t-t_0)^2] \tag{8.8}$$

where future values of $c\Delta t_B$ are predicted based on the coefficients k_0, k_1, and k_2. Thus, over short periods of time the ground and airborne receivers can be considered synchronized. The code phase single difference solution of Eq. 8.2 becomes:

$$\begin{pmatrix} SD^1 - c\Delta\hat{t}_B \\ SD^2 - c\Delta\hat{t}_B \\ \vdots \\ SD^m - c\Delta\hat{t}_B \end{pmatrix} = \begin{bmatrix} e_x^1 & e_y^1 & e_z^1 \\ e_x^2 & e_y^2 & e_z^2 \\ & \vdots & \\ e_x^m & e_y^m & e_z^m \end{bmatrix} \begin{pmatrix} bl_x \\ bl_y \\ bl_z \end{pmatrix} \tag{8.9}$$

where $m \geq 3$ in order to solve the equation.

8.2.2.2 Code Single Difference Solution Using Carrier Assisted Clock Aiding

Here we propose to take advantage of the relatively noise-free carrier phase measurements in order to estimate k_1 and k_2 in Eq. 8.8. This represents a novel approach, and is accomplished using a carrier phase propagation technique to determine how the clock state $c\Delta t_B$ changes over time.

In carrier phase propagation, we start with the change in the single differences from t_1 to t_2:

$$\begin{aligned} \underline{\boldsymbol{SD}}_2 - \underline{\boldsymbol{SD}}_1 &= H_2 \underline{\boldsymbol{bl}}_{c2} - H_1 \underline{\boldsymbol{bl}}_{c1} \\ &= H_2 (\underline{\boldsymbol{bl}}_{c1} + \Delta \underline{\boldsymbol{bl}}_c) - H_1 \underline{\boldsymbol{bl}}_{c1} \end{aligned} \tag{8.10}$$

where $\underline{\boldsymbol{bl}}_c$ is the baseline plus clock vector of Eqs. 8.2-8.3. The left hand side uses the same single difference at two consecutive epochs. Notice that the integer ambiguity term, which is constant for each single difference (Eq. 3.14), cancels when Eq. 8.10 is applied. Also note that the H matrices used here are as described in Eq. 8.2 and are not the differenced direction cosines used when dealing with double differences (see Eq. 8.6). Solving for $\Delta \underline{\boldsymbol{bl}}_c$ we get:

$$\Delta \underline{\boldsymbol{bl}}_c = (H_2^T H_2)^{-1} H_2^T \left[(\underline{\boldsymbol{SD}}_2 - \underline{\boldsymbol{SD}}_1) + H_1 \underline{\boldsymbol{bl}}_{c1} \right] - \underline{\boldsymbol{bl}}_{c1} \tag{8.11}$$

which yields the baseline at t_2:

$$\underline{\boldsymbol{bl}}_{c2} = \underline{\boldsymbol{bl}}_{c1} + \Delta \underline{\boldsymbol{bl}} \tag{8.12}$$

Implicit in this solution is the requirement that H_2, the geometry at t_2, be known. This requires an

estimate of $\underline{\boldsymbol{bl}}_2$ ($\underline{\boldsymbol{bl}}_{c2}$ is not necessary) on which an approximate H_2 calculation is based. This could be accomplished by carrying forward a code double difference solution which is the least squares solution of Eq. 8.7. The initial clock bias, $c\Delta t_{B0}$ could be set to zero since only the change over time (characterized by k_1 and k_2) is desired here and not the clock bias (k_0).

When the clock polynomial is formed, the resulting clock drift over time found from Eq. 8.12 can be used to form an initial clock polynomial. This yields a completely erroneous k_0 term, but a much more accurate estimation of k_1 (clock velocity) and k_2 (clock acceleration). To get k_0 (clock bias), the clock drift of Eq. 8.12 is subtracted from $c\Delta t_B$ as found from Eq. 8.3. The mean of the result is used as k_0. Thus, k_1 and k_2 are found from relatively noise-free carrier phase measurements and k_0 is estimated from noisy code phase measurements. However, this estimate gets better over time as more measurements are used. Once the polynomial is found, the clock difference between the ground and air (including hardware variations), $c\Delta t_B$, can be predicted using (k_0, k_1, k_2) and navigation may proceed using Eq. 8.9.

8.3 Atlantic City Flight Test

8.3.1 Flight Test Description

The flight test was conducted on February 20, 1995 at the FAA Tech Center in Atlantic City, NJ. The airborne platform was a Boeing 757-B which was provided by the United Parcel Service. Three approaches were made to runway 13 at Atlantic City International Airport. The Ashtech Z-12 receivers were augmented by rubidium oscillators and there was no temperature control. The preceding section covered the various DGPS solutions that are presented here to evaluate the navigation performance with clock aiding. Again, the ambiguity-resolved widelane solution from the PNAV software is assumed to represent the true aircraft position. This truth reference is used as a basis of comparison for the other DGPS solutions. It should be noted that the PNAV position was calculated using six satellites although some of the other DGPS solutions were based on fewer than six satellites.

The ground track for the flight is shown in Fig. 8.1. The ground track begins during a turn to the downwind leg for runway 13. The first of the three approaches was not recorded properly because the airborne receiver was set to collect data once every 20 s. This problem was corrected mid-flight by setting the airborne receiver to collect data once per second.

An altitude plot is depicted in Fig. 8.2, which shows the height of the aircraft relative to the ground station. Thus, when the aircraft lands the altitude is not zero but represents a vertical offset between the runway and the ground station. The two highlighted final approach legs took about 3 minutes each, and represent the primary flight data to be used in this analysis.

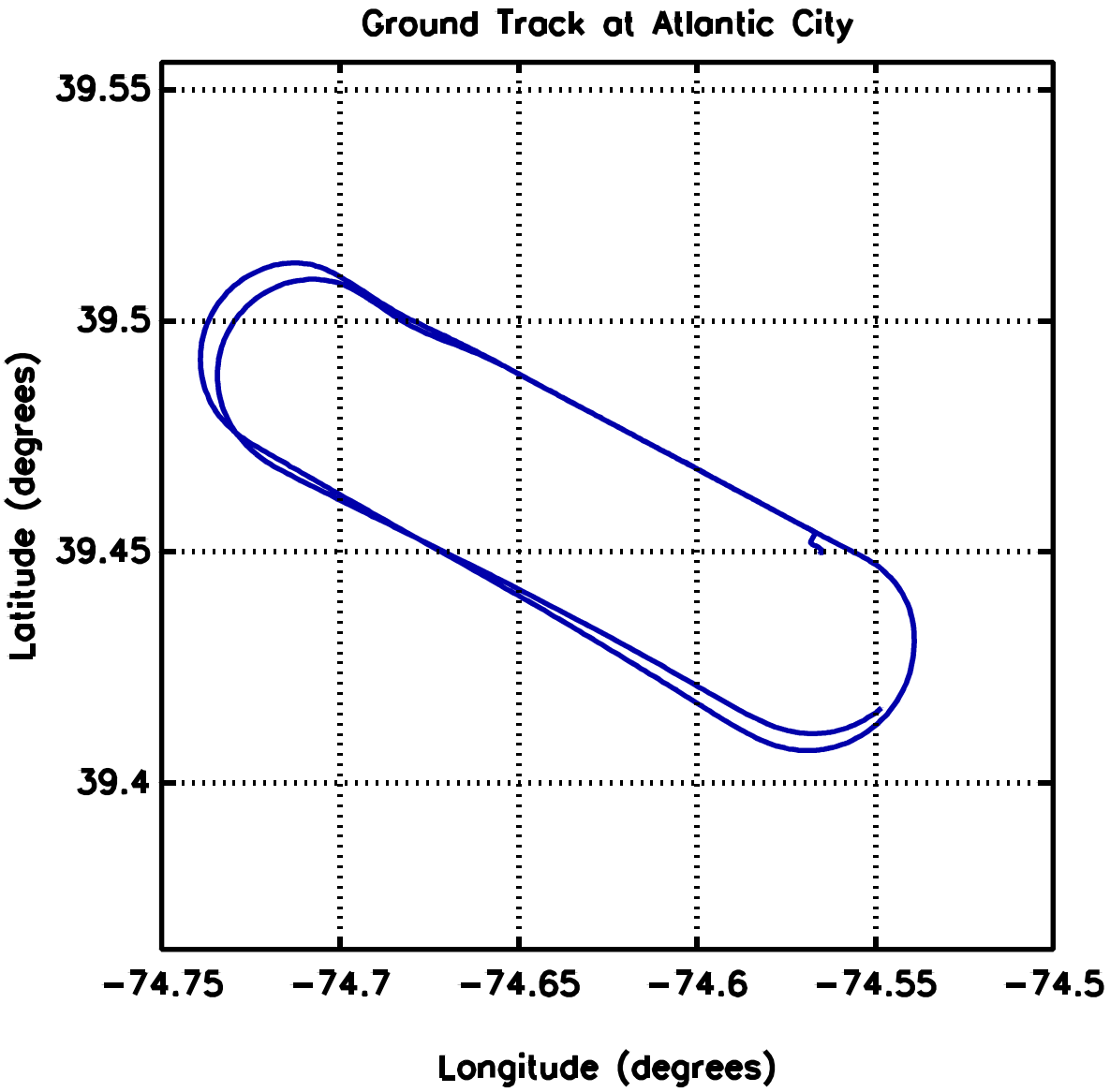

Figure 8.1 Ground Track for Atlantic City Flight Test

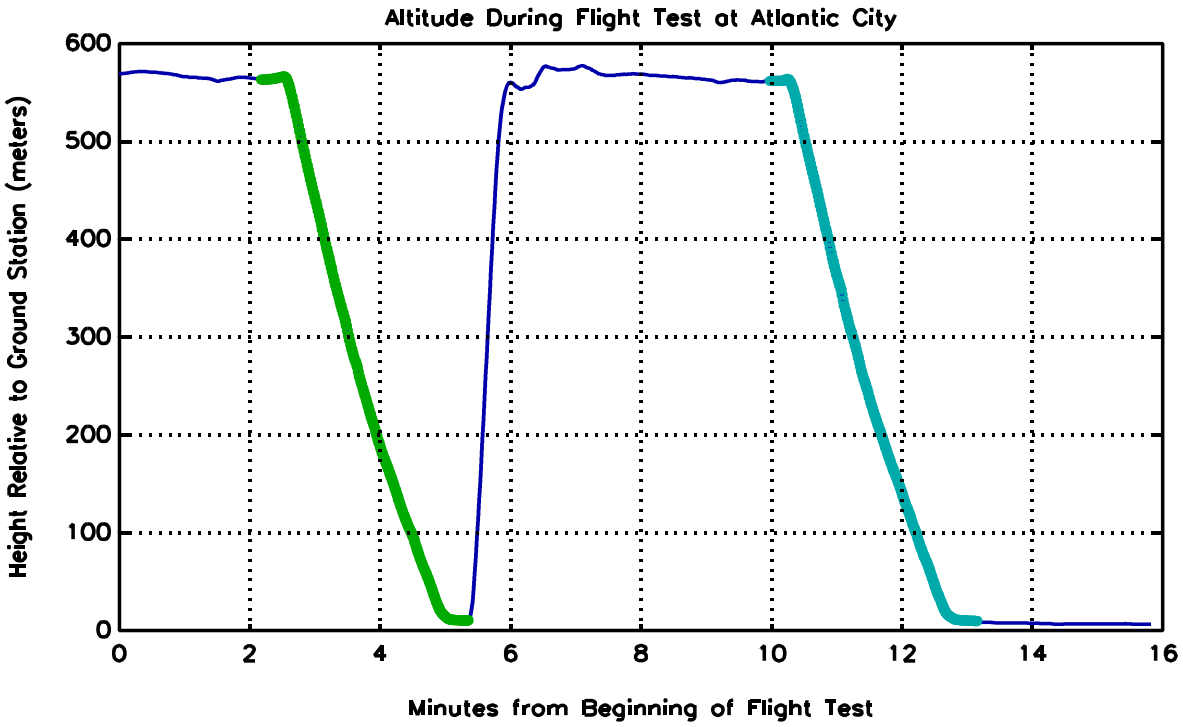

Figure 8.2 Height Above Ground Station During Flight Test at Atlantic City

8.3.2 Clock Bias During the Flight Test at Atlantic City

A clock-aided solution relies on synchronization between air and ground receivers. The drift between the rubidium oscillators was determined during a zero baseline test to be about 1.3 cm/s (see Fig. 6.11), though this could be calibrated. Hardware variations were limited during that test by immersing the receivers in ice baths. During the flight test at Atlantic City, receiver temperature was not controlled. Temperature related hardware drifts were shown in Chapter 6 to be on the order of 10 meters and are not necessarily easy to predict. Thus, the relative clock drift $c\Delta t_B$ between the ground and air receivers includes multiple effects. Two methods were used to determine $c\Delta t_B$ during the flight test, one involving single difference residuals and one involving a carrier phase propagated solution as described in Sec. 8.2.2.2.

First, the single difference residuals were calculated. We begin with the measured single differences for all satellites, each of which contains $c\Delta t_B$, but vary on the order of kilometers as the airplane traces the ground track shown in Fig. 8.1. Thus, a set of reference single differences are needed for comparison in order to observe hardware variations on the order of 10 meters or less. Using the PNAV solution and satellite positions as calculated from the broadcast orbital parameters, the reference single differences can be determined as follows:

$$SD_{true} = R_{gnd} - R_{air} - t_{cor} \tag{8.13}$$

where: SD_{true} is the reference single difference (m)
R_{gnd} is the range from the ground station to the satellite (m)
R_{air} is the range from the aircraft to the satellite (m)
t_{cor} is the correction of Eq. 8.4 (m)

R_{gnd} is based on satellite positions according to the ground station, and R_{air} is based on satellite positions according to the aircraft. These satellite positions are different because the times of transmission of simultaneously received signals are different. This is accounted for in the t_{cor} correction. Thus, a set of reference single differences is calculated by Eq. 8.13, none of which contains $c\Delta t_B$.

Each measured carrier phase single difference contains an integer ambiguity term (ΔN^i) which is different for each satellite. A nominal estimate of each ambiguity is found assuming $c\Delta t_B$ is zero. While this assumption is not true, it simply allows for a direct comparison of the single difference residuals on the same scale. An accurate estimate of $c\Delta t_B$ is reserved for the unambiguous code single difference solution. Thus, the ambiguities are found as:

$$\Delta N = round\left(\frac{1}{\lambda_{L1}} [SD_{meas} - \underline{\boldsymbol{e}} \cdot \underline{\boldsymbol{bl}}_{true}] \right) \tag{8.14}$$

where: SD_{meas} is the measured single difference
$\underline{\mathbf{e}}$ is a direction cosine vector to the satellite
$\underline{\mathbf{bl}}_{true}$ is the baseline according to the PNAV solution

The final step is to simply subtract the reference single difference from the measured single difference in order to get a residual. For a particular satellite:

$$res_{SD} = SD_{meas} - \Delta N \lambda_{L1} - SD_{true} \tag{8.15}$$

which is plotted for each satellite in Fig. 8.3. In a period of 16 minutes, $c\Delta t_B$ changes by about 3 meters. Note that we have not yet determined the relative clock bias, but Eq. 8.15 yields an

estimate of how the receiver clocks drift relative to one another during the flight. This represents a combination of the 1.3 cm/s relative drift between the rubidium oscillators, as well as temperature related hardware variations. It appears that the two effects counteract one another because the clocks should differ by 13 meters after 1000 seconds (~17 minutes) based on the relative rubidium drift alone. The hardware variations are opposite in sign to the rubidium drift, and therefore diminish the amount of drift seen in Fig. 8.3. The residuals do not track each other identically because although $c\Delta t_B$ is a common error, other errors such as residual troposphere delay remain. In other words, the double differences would not be identically zero. The troposphere model is based on standard temperature, barometer, and humidity and is thus not perfect. Noise and multipath errors are also not common between the ground and air receivers.

Fig. 8.4 shows the clock drift as solved for in the single difference carrier phase propagated solution of Eqs. 8.11-12. This clock drift matches very closely the single difference residuals of Fig. 8.3. Thus, Fig. 8.4 represents a relatively noise free illustration of clock velocity, acceleration and higher order terms during the flight test. This curve is obtained in real-time and can be used to estimate k_1 and k_2 in the clock polynomial of Eq. 8.8.

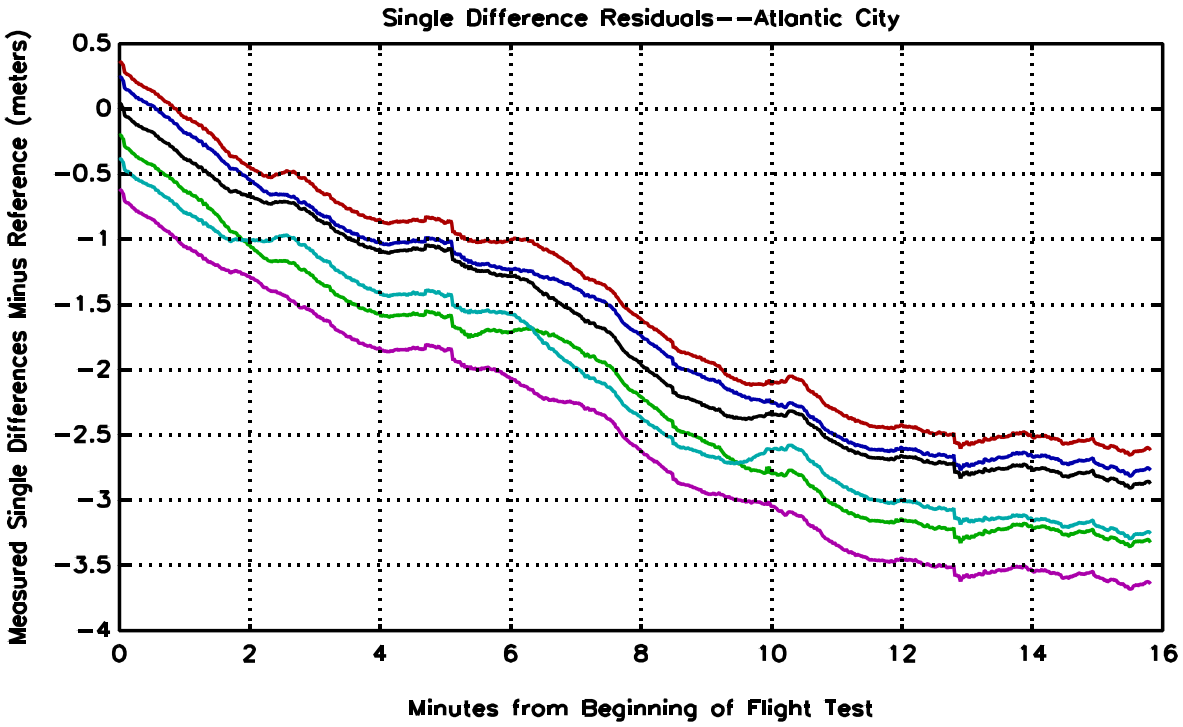

Figure 8.3 Single Difference Residuals During Flight Test at Atlantic City for SVs 1 6 14 20 22 25

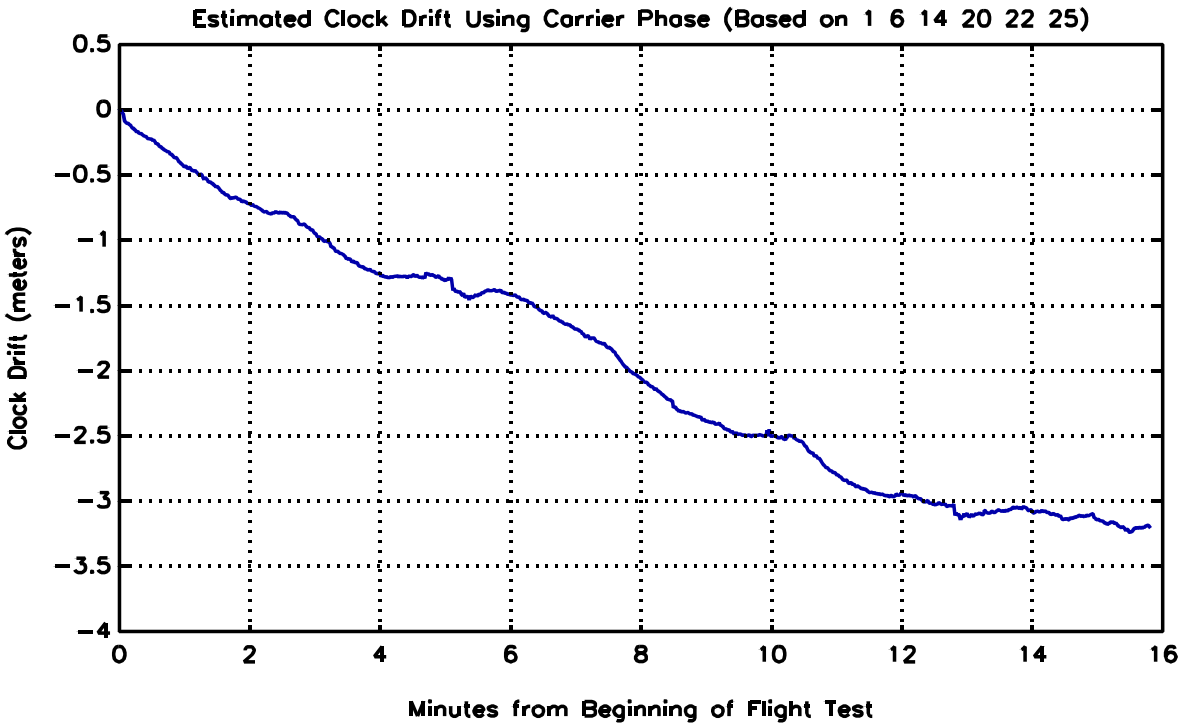

Figure 8.4 Clock Drift Based on Carrier Phase Propagation — Atlantic City

8.3.3 Comparison of Standard and Carrier-Assisted Clock Modeling

The standard clock model is formed by solving Eq. 8.2 and observing $c\Delta t_B$ over time. The clock drift of Fig. 8.4 can be used to enhance this model. Here we compare the standard and carrier-assisted clock polynomials at four different points during the flight test — the beginning and end of each approach. This allows for a comparison as a function of how much prior data is used for modeling $c\Delta t_B$.

Fig. 8.5 shows $c\Delta t_B$ as calculated using the code single difference solution (Eq. 8.2), along with the two clock estimates. Note that the noisy clock state is the data on which the standard clock model is based. The carrier-assisted clock model uses the same segment of data before Approach 1 (approximately two minutes) but also uses the carrier-based clock drift (Fig. 8.4). Thus, the clock polynomials (k_0, k_1, k_2) are formed at the beginning of the first approach, and Fig. 8.6 shows the error growth in the two models after that point. Because the exact value of $c\Delta t_B$ at that point is unknown, it is assumed in Fig. 8.6 that the initial offset from the true $c\Delta t_B$ is zero for each model. The true clock drift from that point forward (approximately 14 minutes of data) is taken from Fig. 8.4 and is used as a reference for the error growth shown in Fig. 8.6. Thus, we see that the carrier assisted clock model outperforms the standard clock model.

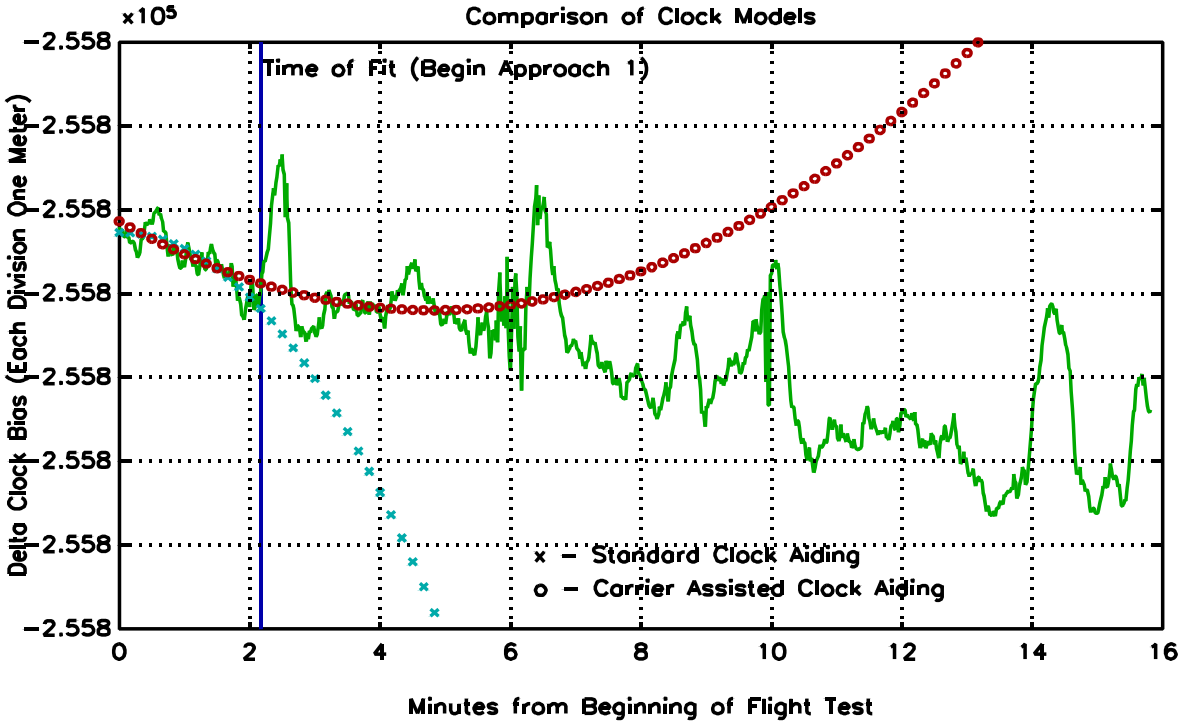

Figure 8.5 Comparison of Clock Predictions at Beginning of Approach 1

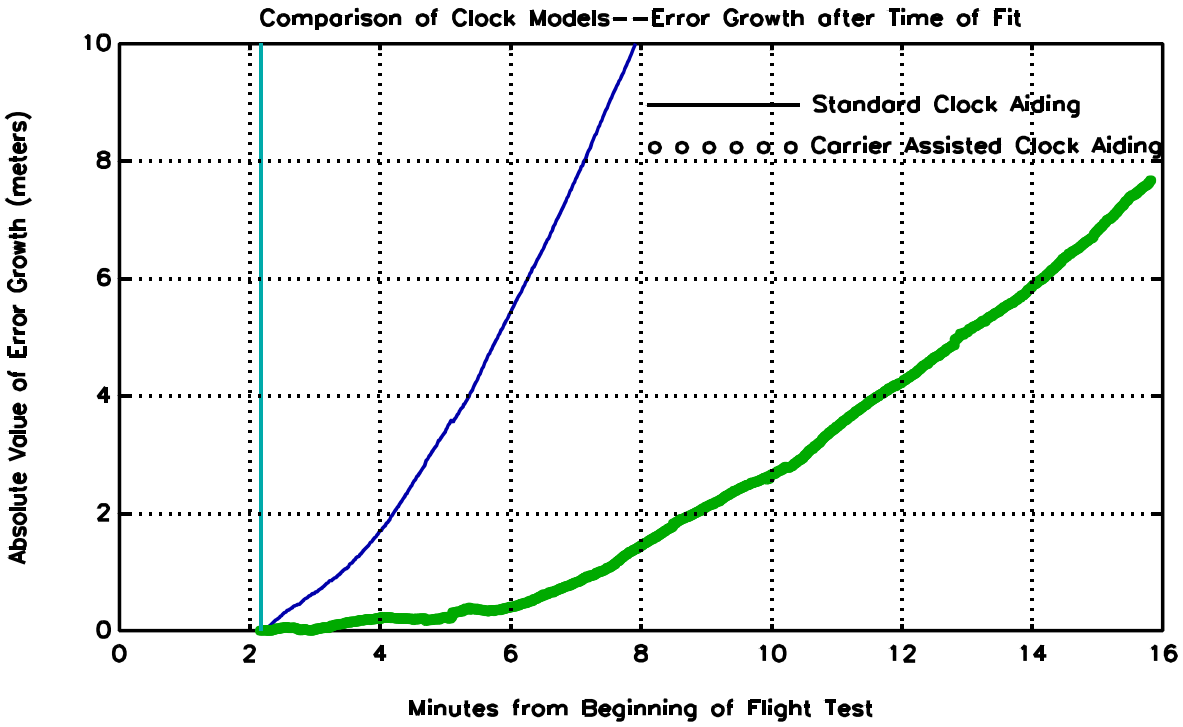

Figure 8.6 Error Growth in Clock Predictions Using Clock Polynomials from the Beginning of Approach 1

Figs. 8.7-8.12 illustrate similar cases but with the clock models formed at later points in the data. We see that for the most part, the carrier-assisted clock model is better than the standard clock model. However, as time goes on, the standard clock model gets better because it is based on increased amounts of prior data. One important implication is that carrier phase should be used in order to get a quicker fix on a good clock model. Furthermore, the carrier-assisted clock model is able to follow quick changes in the clock offset without filtering delays. Figs. 8.5-8.12 also give an idea of how long one can expect to coast on the clock and maintain an accurate position solution. A more extensive analysis could be performed to define a time limit after which the clock should not be used. It should be noted that as long as at least four satellites are available, the clock polynomial coefficients can continually be updated. This is the approach used in the following section where we look at position errors for the two clock aiding methods.

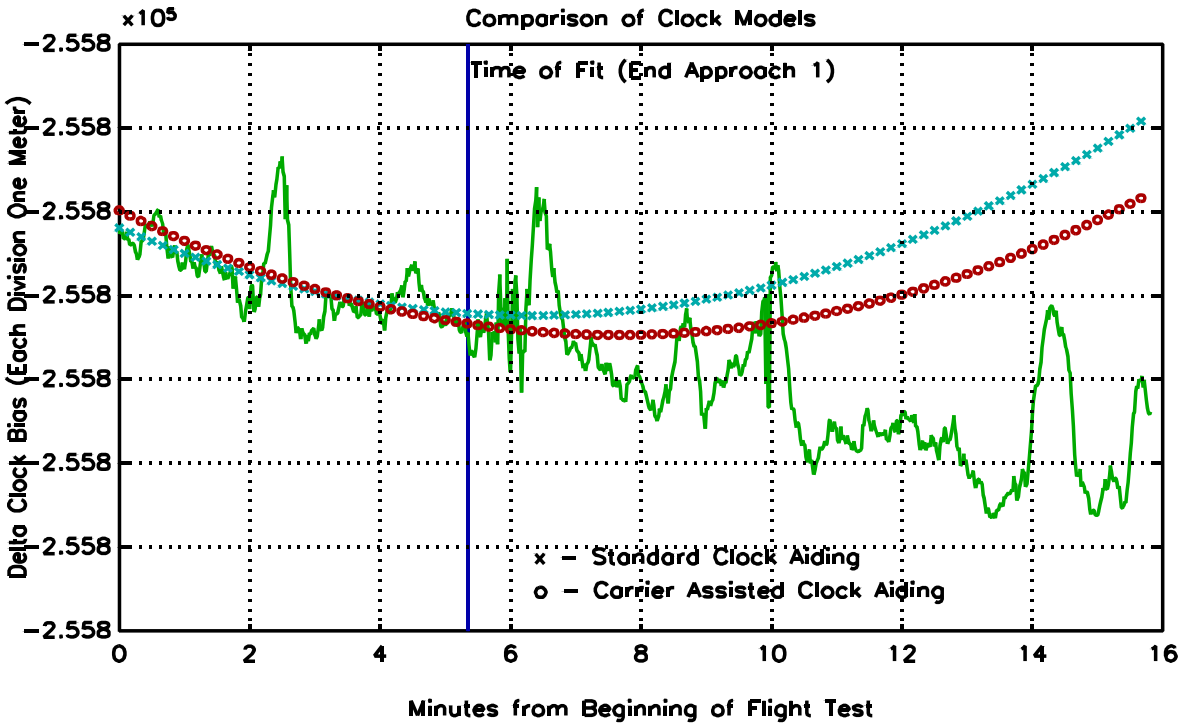

Figure 8.7 Comparison of Clock Predictions at the End of Approach 1

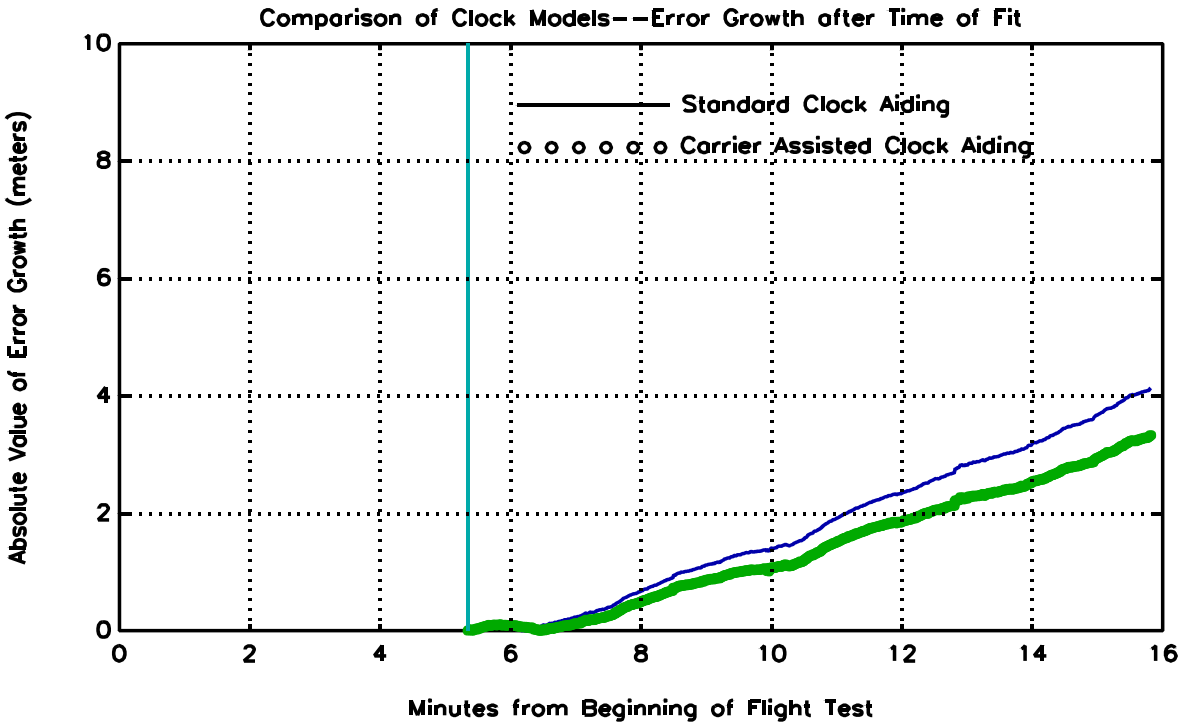

Figure 8.8 Error Growth in Clock Predictions Using Clock Polynomials at the End of Approach 1

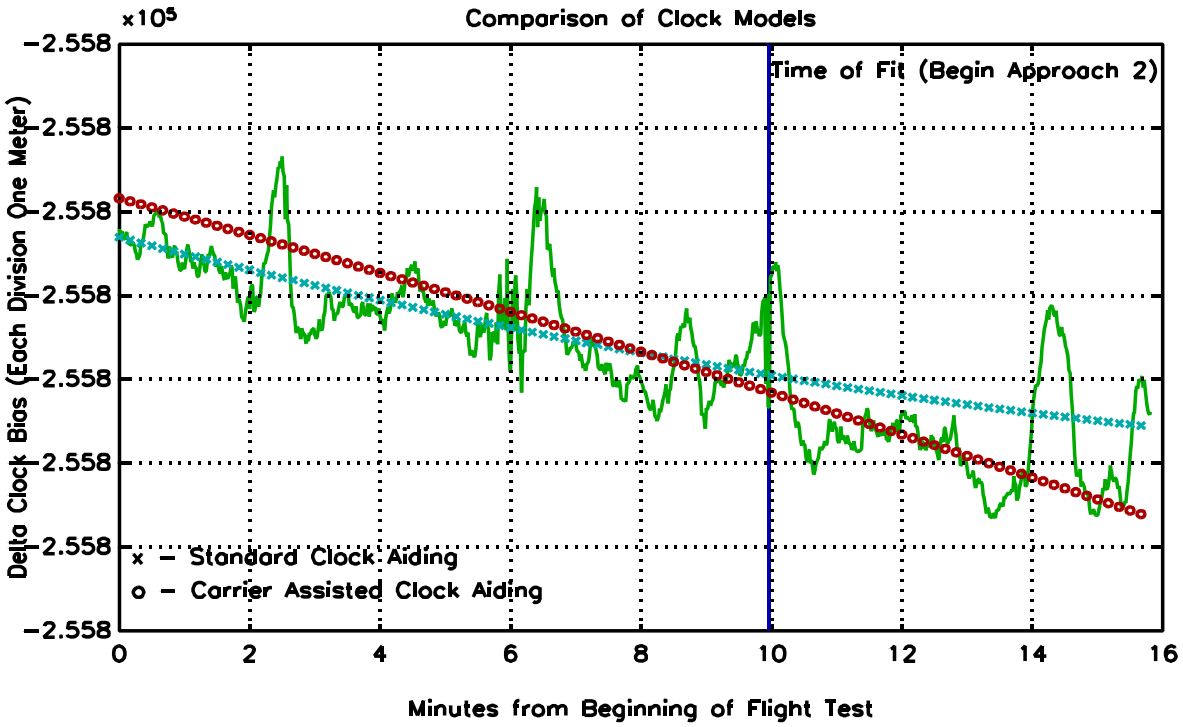

Figure 8.9 Comparison of Clock Predictions at the Beginning of Approach 2

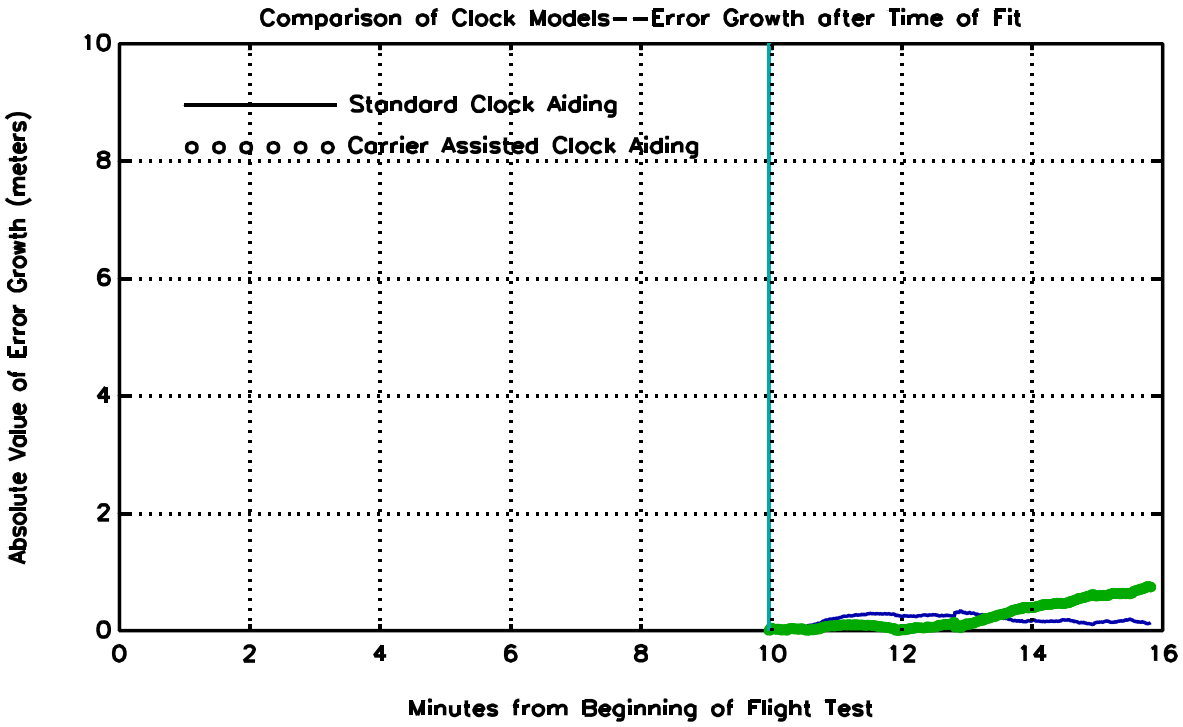

Figure 8.10 Error Growth in Clock Predictions Using Clock Polynomials at the Beginning of Approach 2

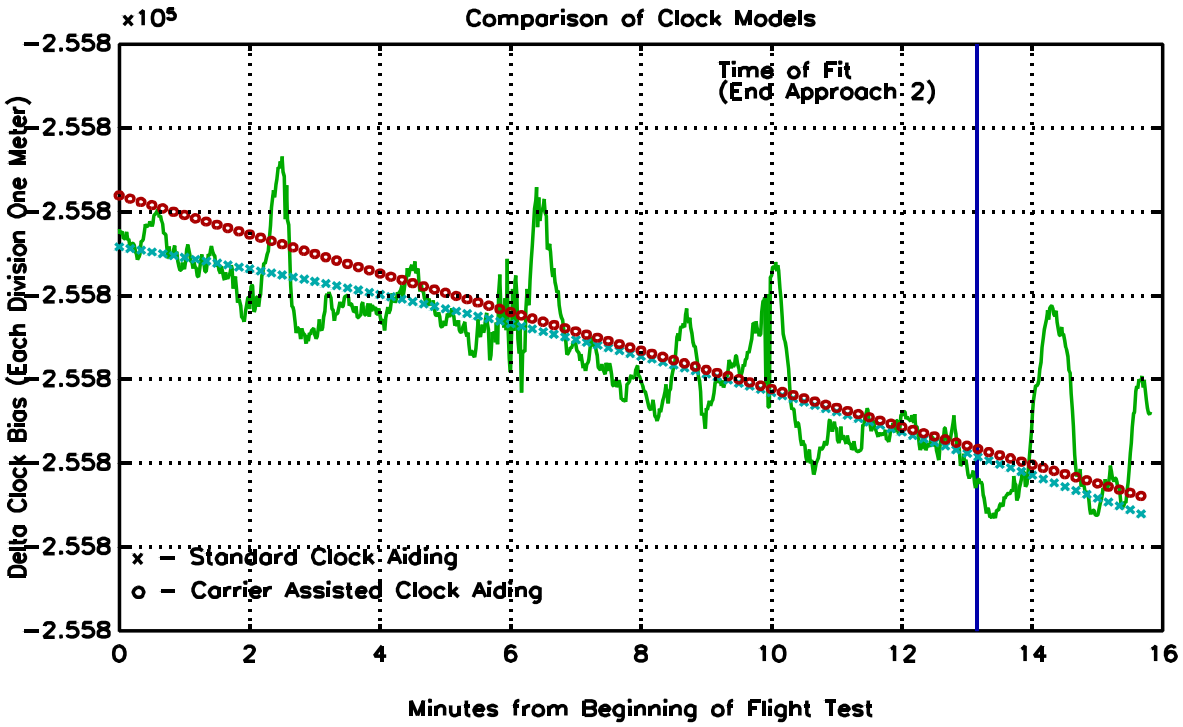

Figure 8.11 Comparison of Clock Predictions at End of Approach 2

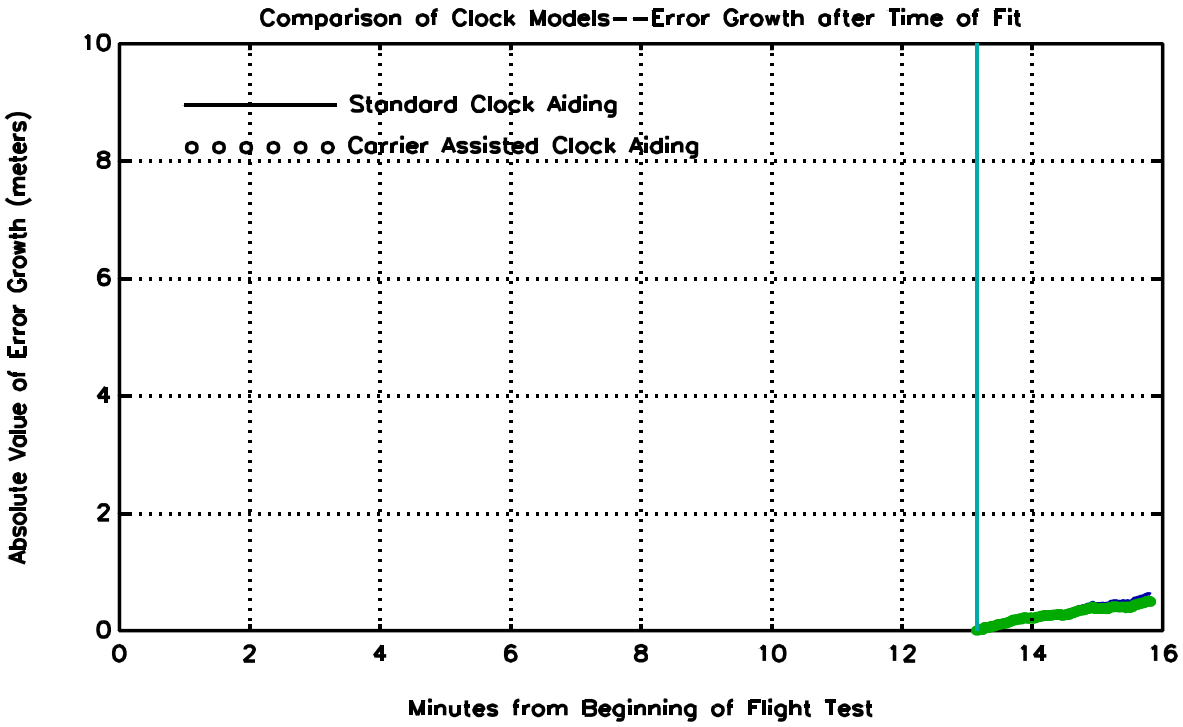

Figure 8.12 Error Growth in Clock Predictions Using Clock Polynomials at the End of Approach 2

8.3.4 Geometry During Atlantic City Approaches 1 and 2

For Approach 1, two scenarios are considered, one using all six satellites and one using a subset of four satellites. The purpose is to show the value of clock coasting, especially during periods of high VDOP. The average horizontal and vertical dilution of precision for each Approach 1 scenario are shown in Table 8.1. The DOPs were calculated using the satellite geometry relative to the ground station. The subset of four satellites was chosen because of the poor VDOP and simulates a circumstance where clock aiding might be used. Here the ground and airborne clocks are assumed to be perfectly synchronized. Thus, the VDOP improvement from clock aiding illustrated in Table 8.1 represents the maximum benefit of clock aiding. In practice, an erroneous clock estimate causes a position error which limits the benefit according to how close the clock model is to the truth.

For Approach 2, there is more history available for the clock models and therefore navigation with three satellites will be demonstrated. Besides the all-in-view case, another scenario with only four satellites (1 6 22 25) is considered. At the beginning of the approach it is assumed that one satellite is lost and that navigation must continue using the remaining three satellites plus the clock. This is done for all four subsets of three satellites. Note that even with three satellites, we get a VDOP improvement over the four satellite case as long as the lost satellite is not a high elevation satellite (SV 25). For the all-in-view geometry, note that the average DOPs are about the same as in Approach 1, which took place about 8 minutes before Approach 2.

Table 8.1 Average HDOP and VDOP During Approach 1 at Atlantic City

	Average HDOP	Average VDOP
SVs 1 6 14 20 22 25	1.13	1.90
SVs 1 6 14 20 22 25 + Clock	1.10	0.68
SVs 6 20 22 25	7.01	9.57
SVs 6 20 22 25 + Clock	1.49	0.83

Table 8.2 Average HDOP and VDOP During Approach 2 at Atlantic City

	Average HDOP	Average VDOP
SVs 1 6 14 20 22 25	1.15	2.06
SVs 1 6 14 20 22 25 + Clock	1.10	0.67
SVs 1 6 22 25	2.43	3.14
SVs 6 22 25 + Clock	1.69	0.89
SVs 1 22 25 + Clock	1.97	0.84
SVs 1 6 25 + Clock	3.16	1.03
SVs 1 6 22 + Clock	5.51	4.79

8.3.5 Position Error Analysis for Atlantic City Approach 1

The offset from the PNAV truth in the vertical direction for each solution is shown in Fig. 8.13 for the all-in-view case, and in the horizontal direction in Fig. 8.14. The clock-aided solutions are initiated at the beginning of the approach by finding the clock polynomial coefficients. These coefficients are updated using new measurements as the approach continues. This explains why the single difference solution with standard clock aiding gets better in terms of vertical accuracy as the approach progresses. The use of carrier phase measurements yields a clock-aided solution that is fairly accurate in the vertical direction at the beginning of the approach.

The unaided code single and double difference solutions are very similar in both horizontal and vertical position error. The vertical accuracy improvement of the clock-aided solutions over the unaided solutions is evident in Fig. 8.13. The horizontal accuracy (Fig. 8.14) shows no substantial improvement when clock aiding is used. This is due to the lack of HDOP improvement for the all-in-view case as seen in Table 8.1.

Figures 8.15-8.16 illustrate the four-satellite case where the VDOP without clock aiding is 9.57 and the HDOP is 7.01. Note the change in scale from the plots in Figs. 8.13-8.14. Here, the position errors are much larger. The benefit of clock coasting is more pronounced due to the poor geometry. Again, the clock polynomial coefficients are continually updated along the approach. Using the carrier phase to assist in the clock modeling provides an improvement over the standard clock model. The unaided solutions are again very similar in terms of position

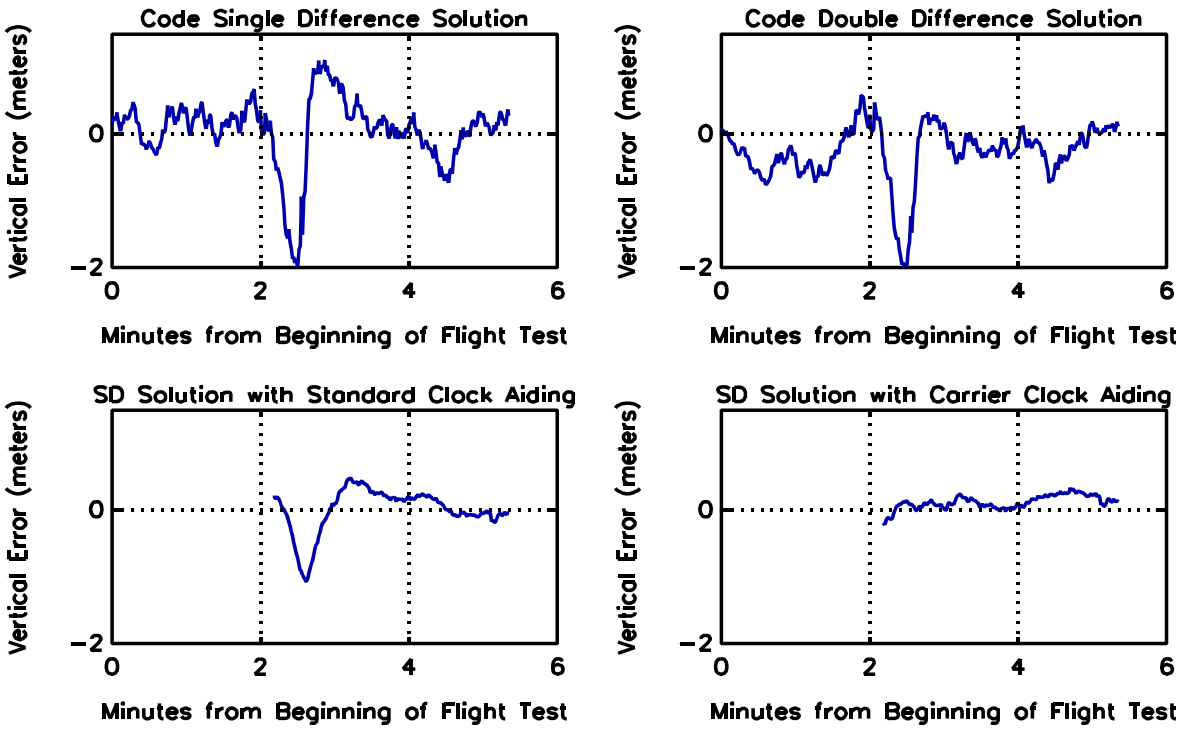

Figure 8.13 Vertical Offset from PNAV Position for DGPS Solutions Through Approach 1 — PNAV Reference Uses SVs 1 6 14 20 22 25, Other Solutions Use SVs 1 6 14 20 22 25

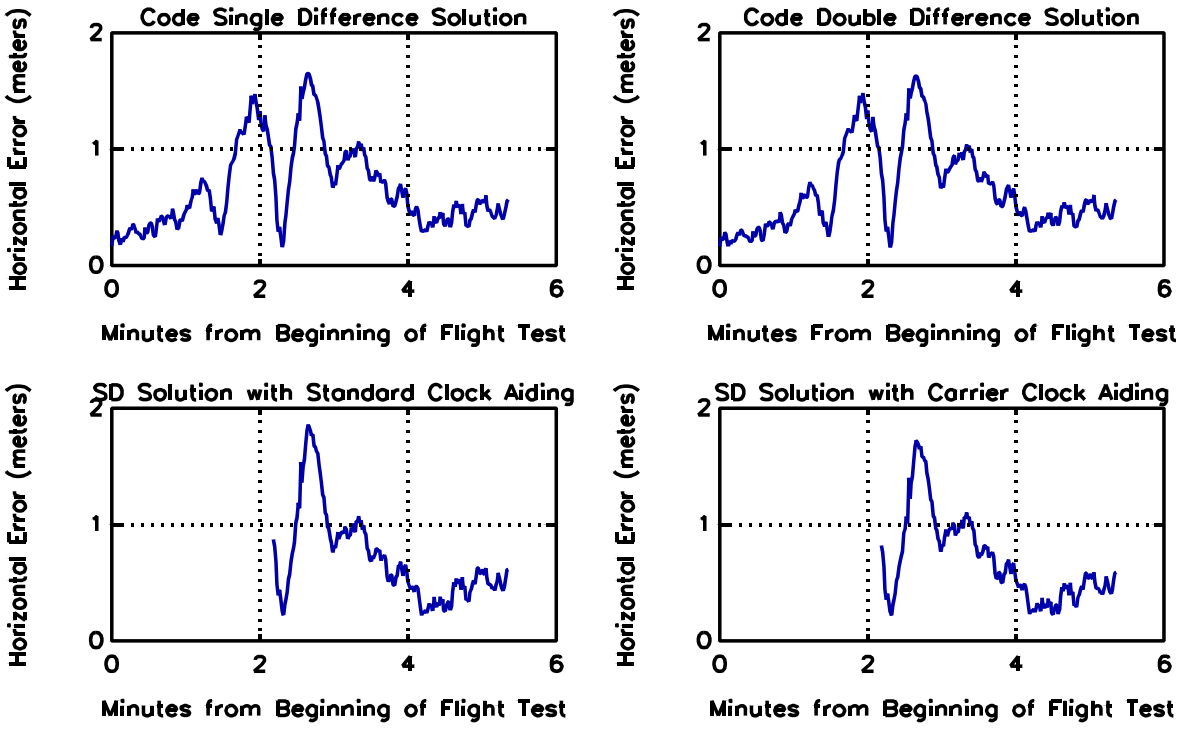

Figure 8.14 Horizontal Offset from PNAV Position for DGPS Solutions Through Approach 1 — PNAV Reference Uses SVs 1 6 14 20 22 25, Other Solutions Use SVs 1 6 14 20 22 25

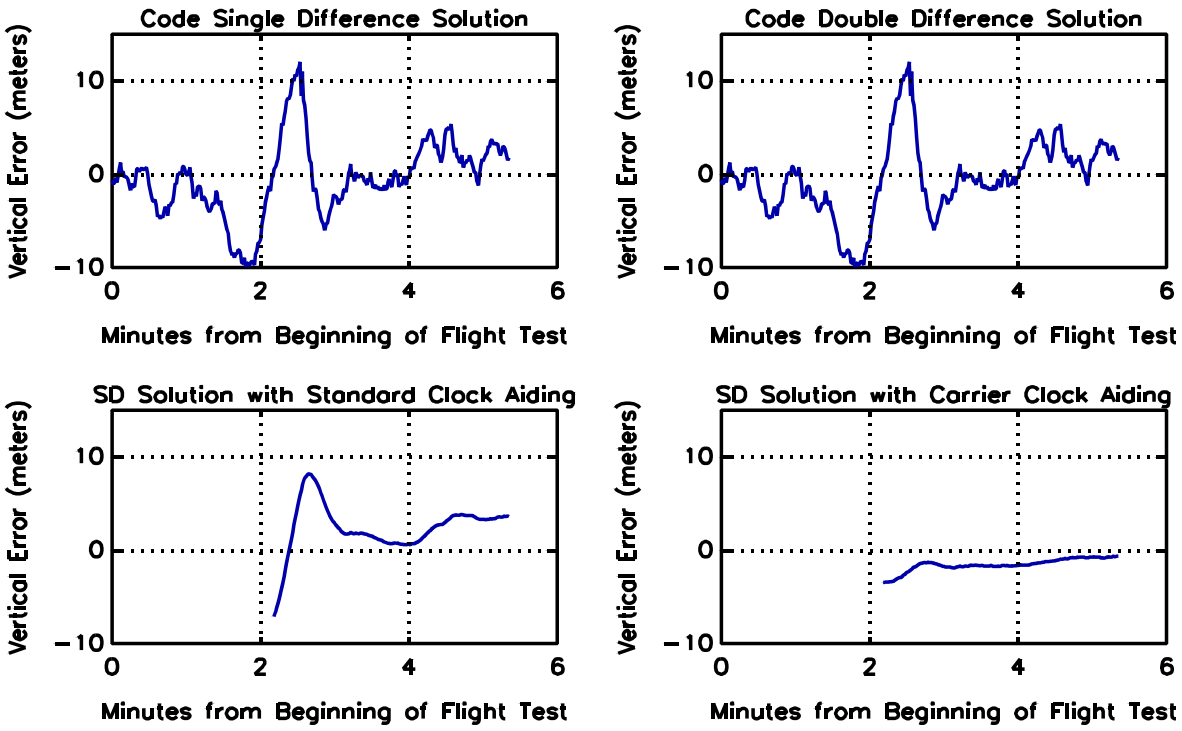

Figure 8.15 Vertical Offset from PNAV Solution for DGPS Solutions Through Approach 1 — PNAV Reference Uses SVs 1 6 14 20 22 25, Other Solutions Use SVs 6 20 22 25

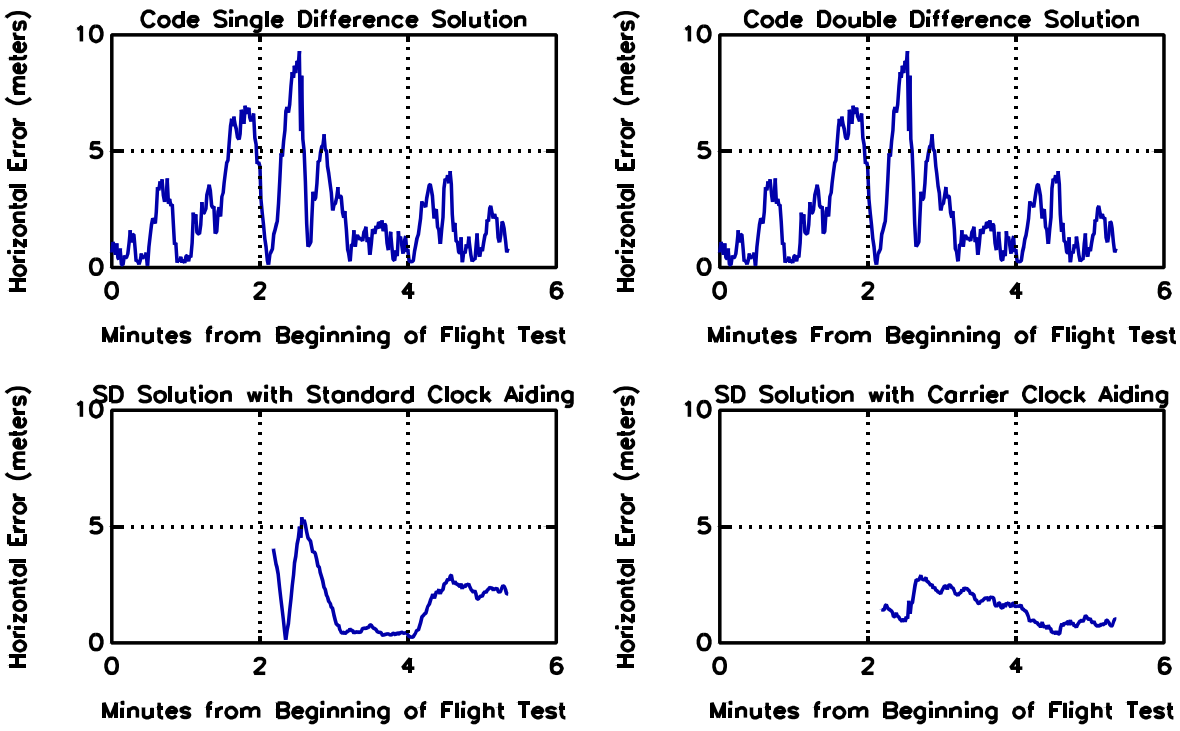

Figure 8.16 Horizontal Offset from PNAV Solution for DGPS Solutions Through Approach 1 — PNAV Reference Uses SVs 1 6 14 20 22 25, Other Solutions Use SVs 6 20 22 25

accuracy. In this scenario, there is also an improvement in horizontal position error when clock aiding is used. This follows from the fact that HDOP is improved from 7.01 to 1.49 (ideally) when clock coasting is used. Thus, if the geometry is poor, clock aiding improves horizontal accuracy as well.

8.3.6 Approach 2 at Atlantic City

The all-in-view vertical and horizontal position errors are shown in Figs. 8.17-8.18 for Approach 2 at Atlantic City. Clock coasting is initiated at the beginning of the approach. In this case, the standard clock model does not exhibit the settling period evident in Figs. 8.13 and 8.15 because here the model is based on ten minutes of prior data. Still, the carrier assisted clock solution appears to be more stable in the vertical direction. The vertical accuracy improvement is again evident for the clock-aided solutions. There is no substantial improvement in the horizontal direction due to the lack of HDOP improvement as shown in Table 8.2.

Next, we look at a four satellite case for Approach 2. Satellites 14 and 20 were eliminated because they yielded erroneous measurements for a few seconds at various points during the flight test. Thus, eliminating these two satellites simulates a failure of these two satellites. We see from Table 8.2 that the geometry is not poor in this case, with an HDOP of 2.43 and a VDOP of 3.14. However, the loss of another satellite would cause HDOP and VDOP to go to infinity without the aid of an additional measurement. Figures 8.19-8.20 show the accuracy in the code single and double difference solutions for the period leading up to Approach 2. The solutions are nearly identical when only four satellites are used.

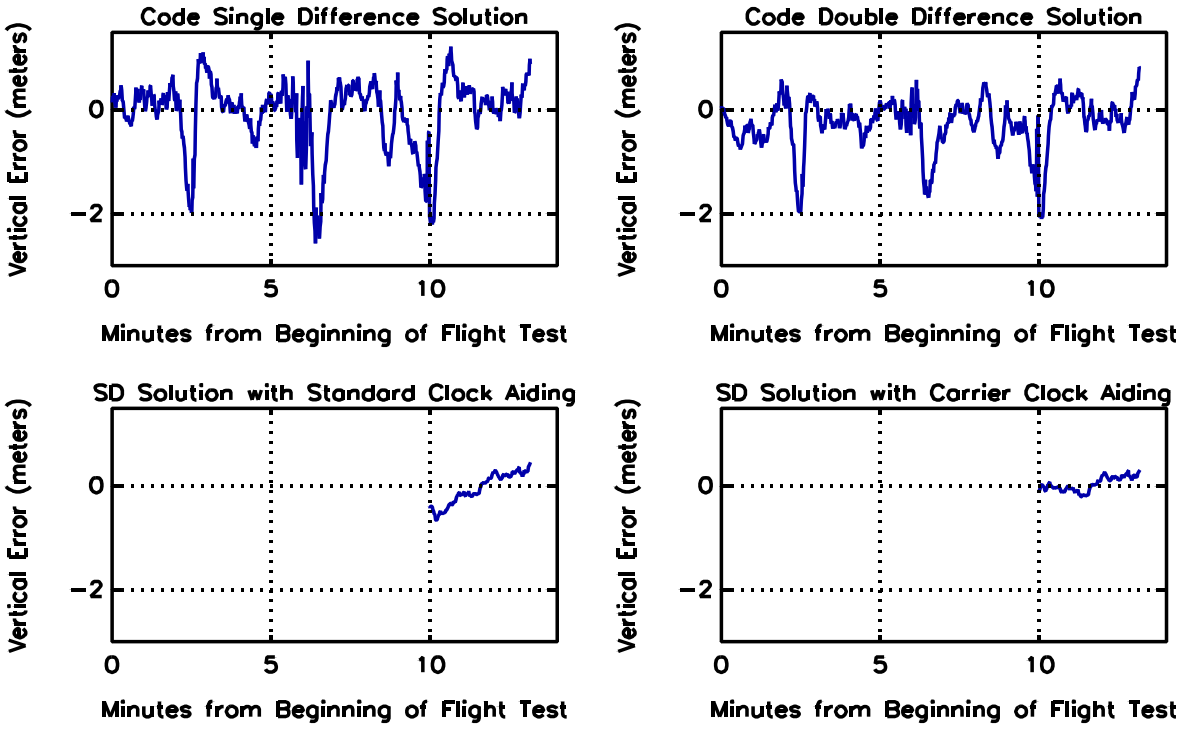

Figure 8.17 Vertical Offset from PNAV Solution for DGPS Solutions Through Approach 2 — PNAV Reference Uses SVs 1 6 14 20 22 25, Other Solutions Use SVs 1 6 14 20 22 25

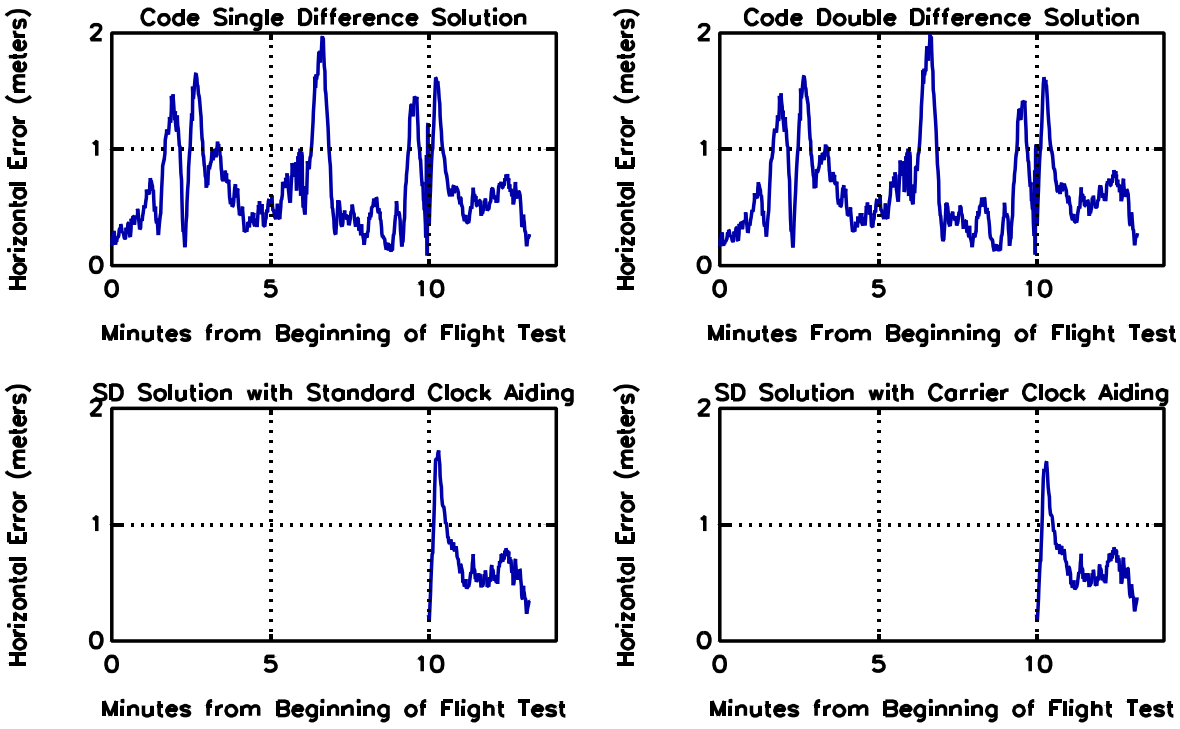

Figure 8.18 Horizontal Offset from PNAV Solution for DGPS Solutions Through Approach 2 — PNAV Reference Uses SVs 1 6 14 20 22 25, Other Solutions Use SVs 1 6 14 20 22 25

Now assume that SV 1 fails, leaving only three usable satellites. We can no longer calculate the unaided code differential solutions. Thus, to continue navigating we must turn to clock aiding. This is depicted in Figs. 8.21-8.22. Here, the clock polynomial coefficients (k_0, k_1, k_2) are fixed at the beginning of Approach 2 because with only three satellites there is not enough information to continue updating the estimate of $c\Delta t_B$. The performance of the carrier-assisted clock model appears slightly better than the standard clock model, though the difference in the horizontal accuracy is more pronounced between the two.

Figures 8.23-8.24 show the performance of the clock-aided solutions when SV 6 is lost and Figures 8.25-8.26 illustrate the scenario where SV 22 is lost. The two clock models appear to provide solutions of similar vertical accuracy, although the carrier-assisted clock aiding does better than the standard model in horizontal accuracy when SV 22 is eliminated.

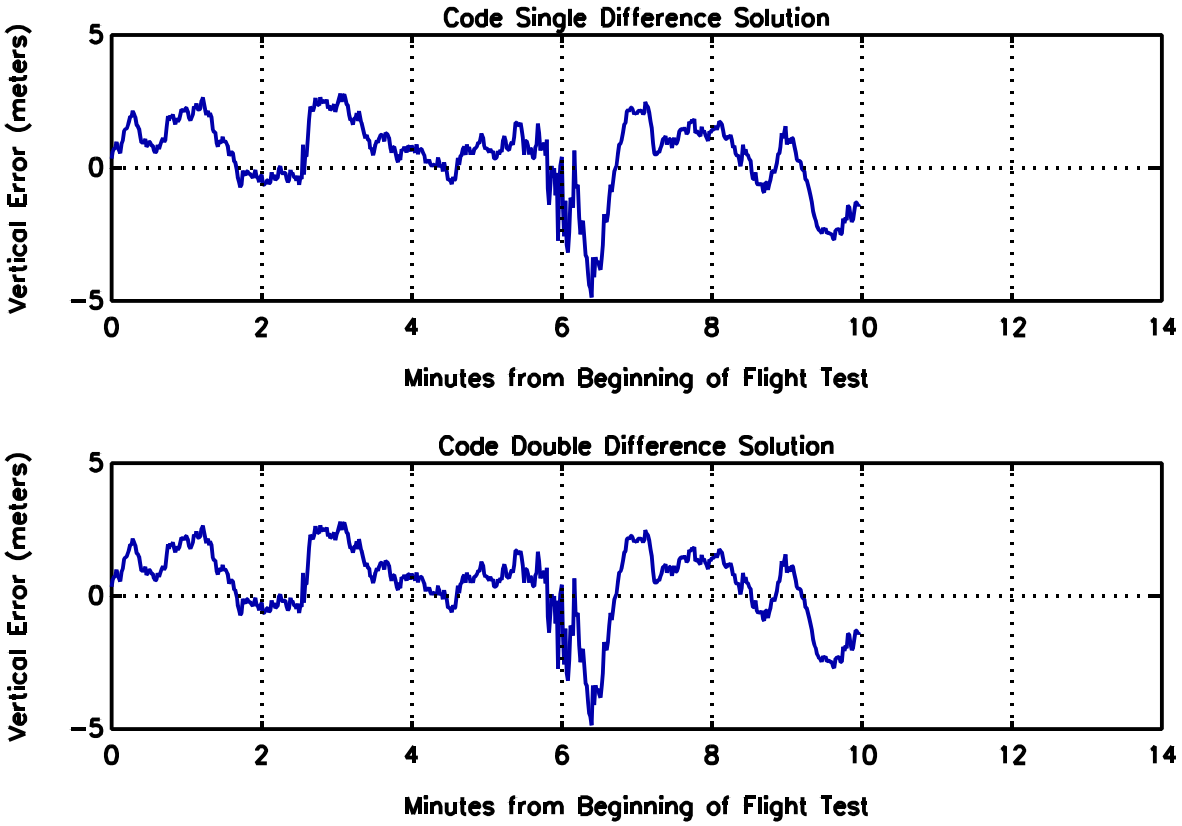

Figure 8.19 Vertical Offset from PNAV Solution for DGPS Solutions up to Start of Approach 2 — PNAV Reference Uses SVs 1 6 14 20 22 25, Other Solutions Use SVs 1 6 22 25

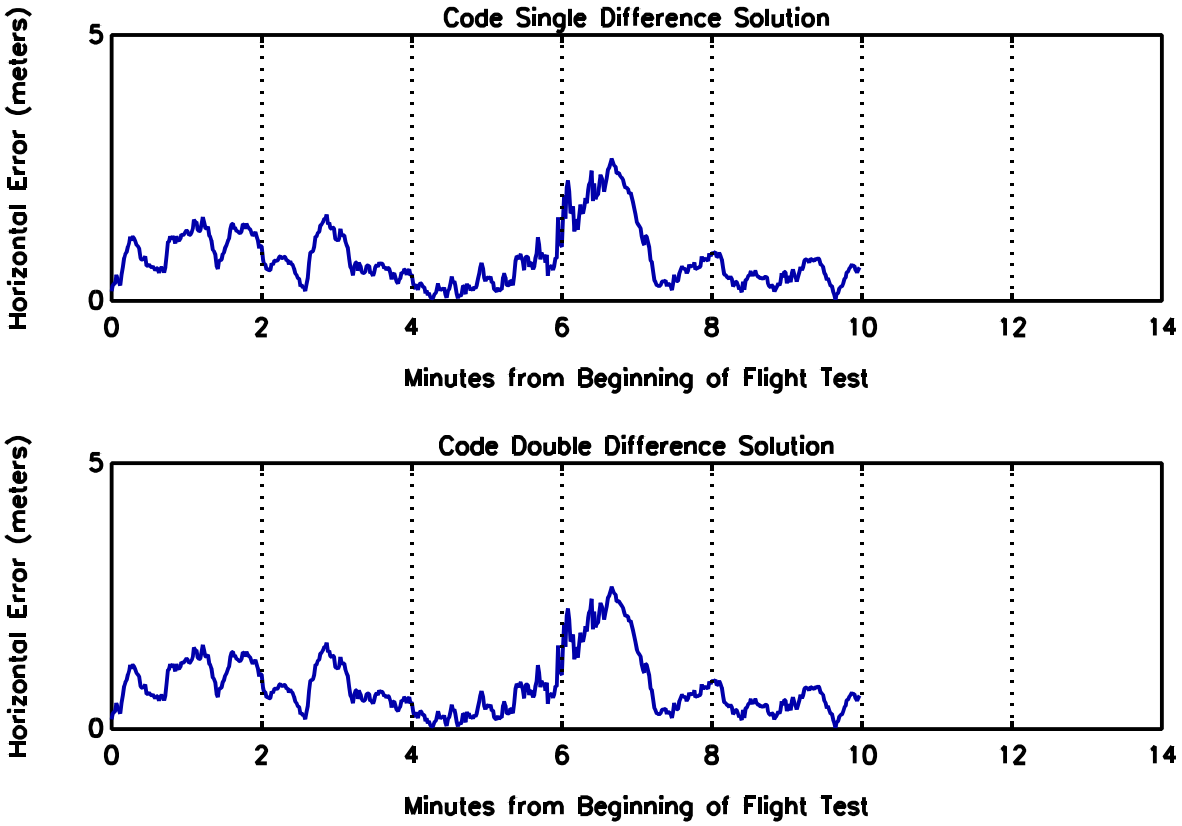

Figure 8.20 Horizontal Offset from PNAV Solution for DGPS Solutions up to Start of Approach 2 — PNAV Reference Uses SVs 1 6 14 20 22 25, Other Solutions Use SVs 1 6 22 25

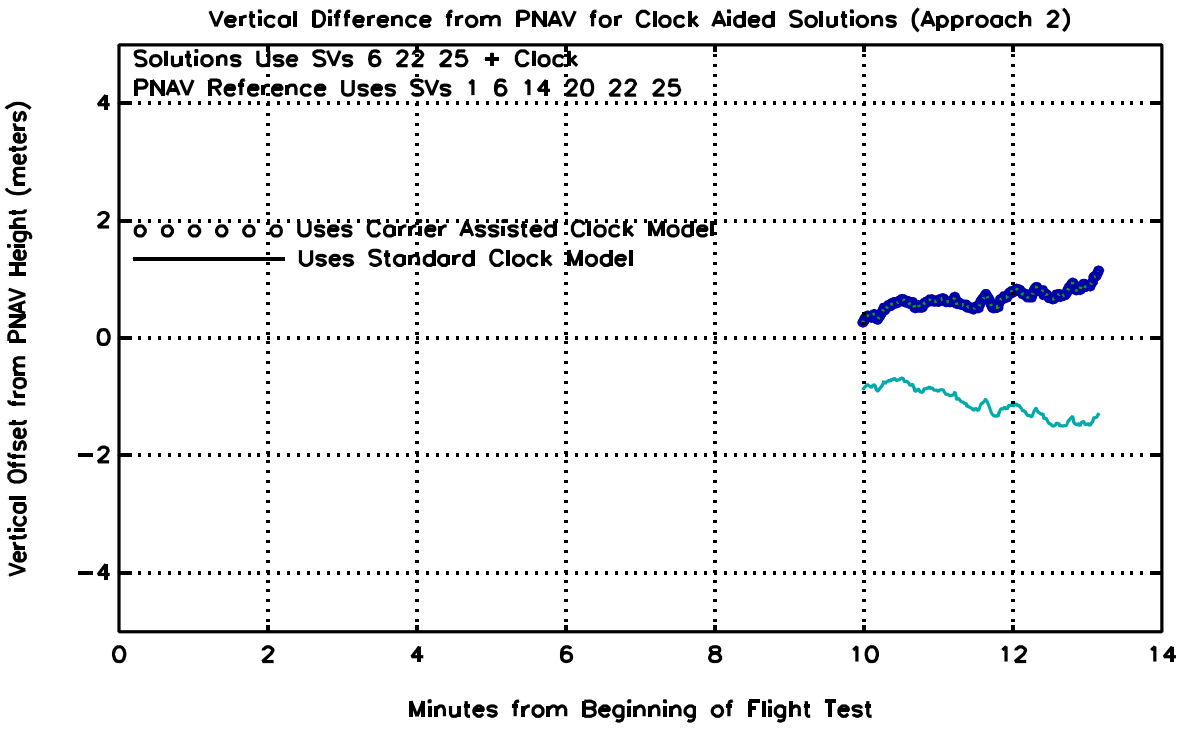

Figure 8.21 Vertical Offset from PNAV Solution for Clock Aided Solutions Using SVs 6 22 25 Plus Clock During Approach 2

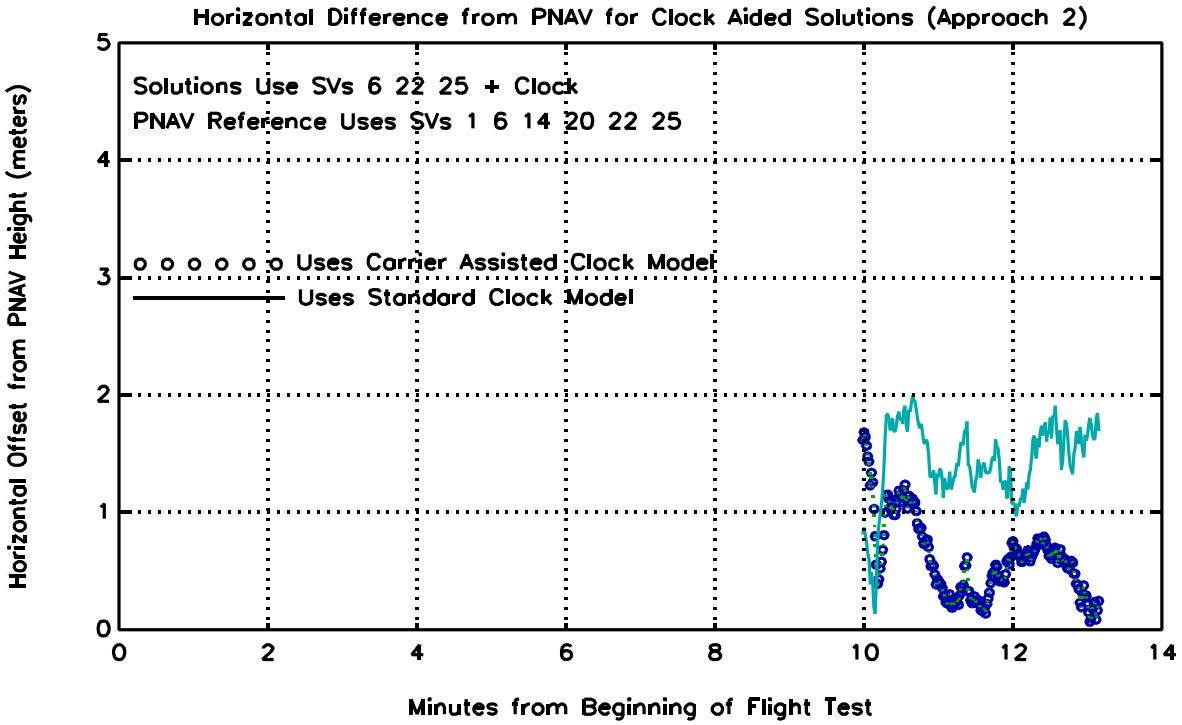

Figure 8.22 Horizontal Offset from PNAV Solution for Clock Aided Solutions Using SVs 6 22 25 Plus Clock During Approach 2

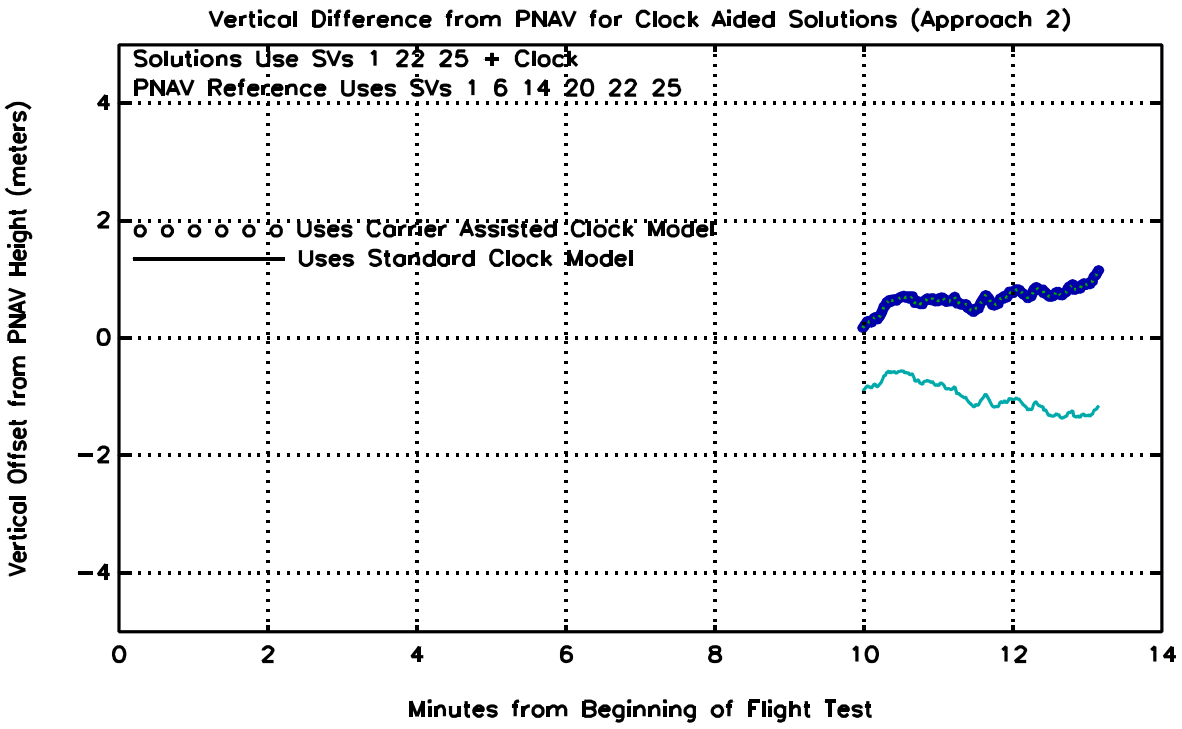

Figure 8.23 Vertical Position Offset from PNAV Solution for Clock-Aided Solutions Using SVs 1 22 25 Plus Clock During Approach 2

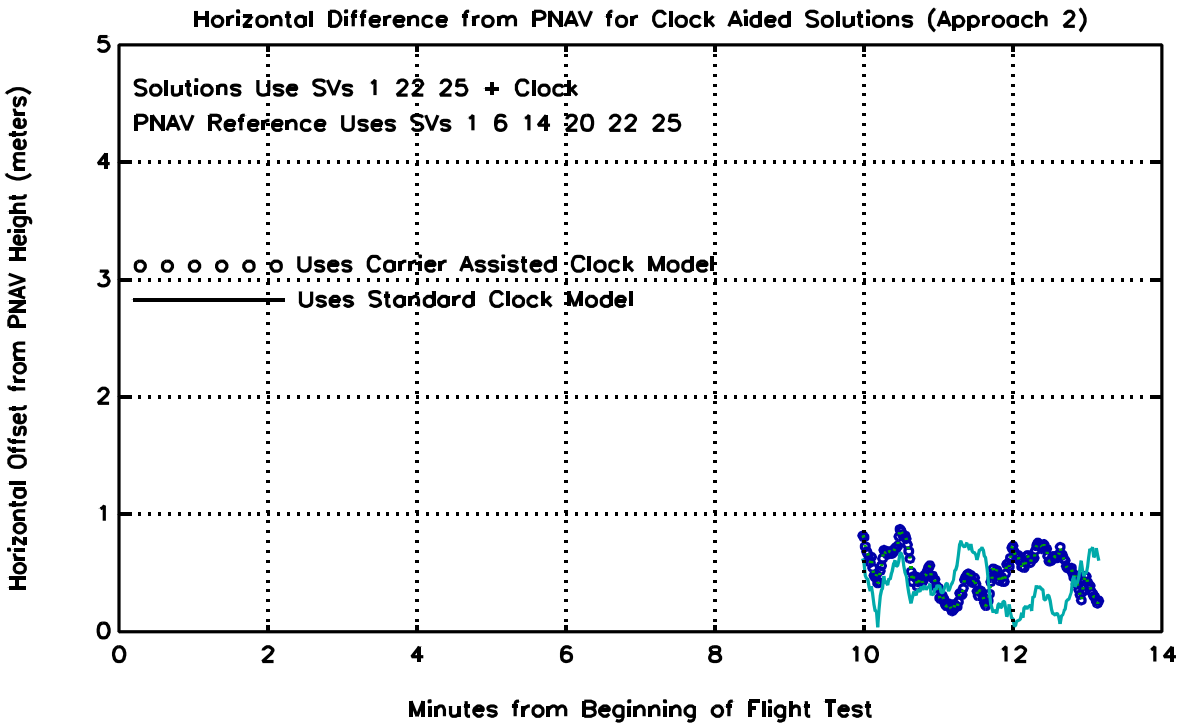

Figure 8.24 Horizontal Offset from PNAV Solution for Clock Aided Solutions Using SVs 1 22 25 Plus Clock During Approach 2

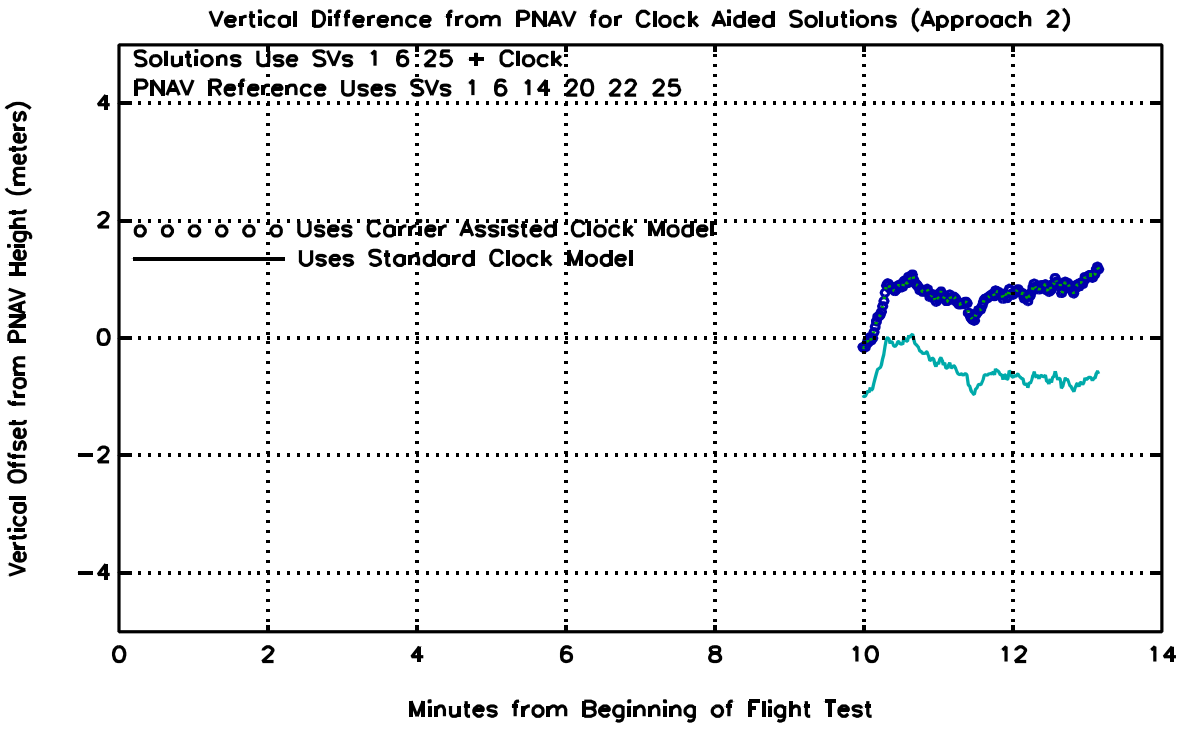

Figure 8.25 Vertical Offset from PNAV Solution for Clock Aided Solutions Using SVs 1 6 25 Plus Clock During Approach 2

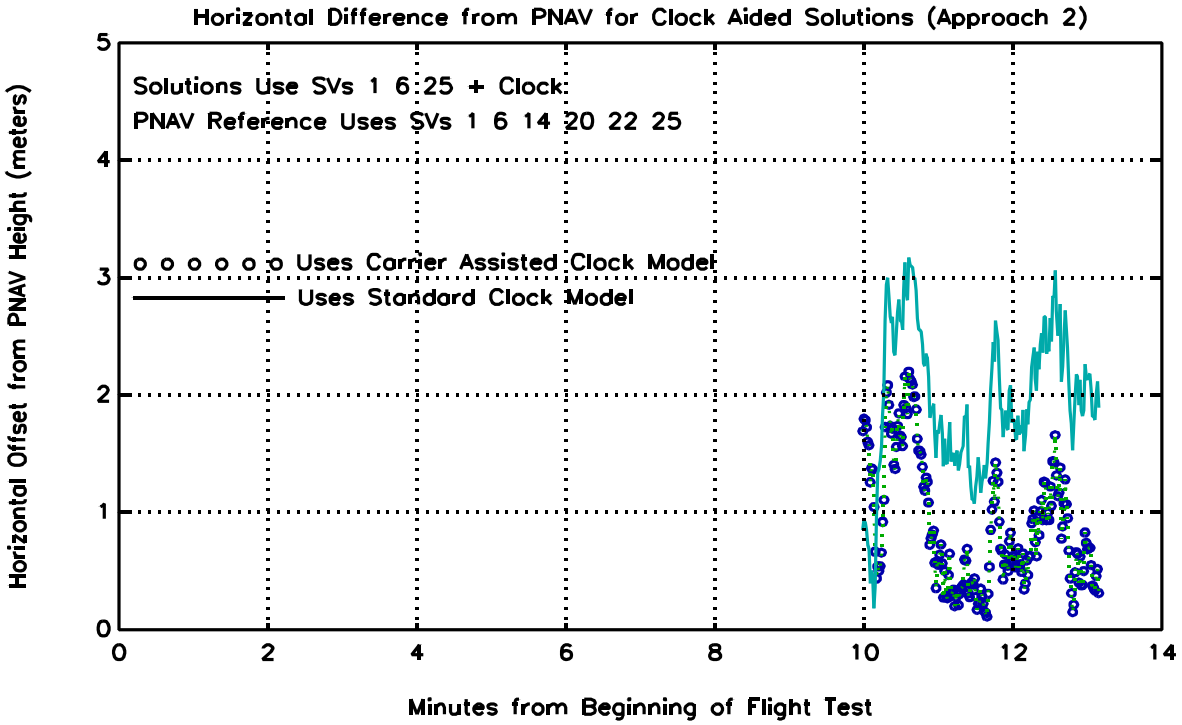

Figure 8.26 Horizontal Offset from PNAV Solution for Clock Aided Solutions Using SVs 1 6 25 Plus Clock During Approach 2

Finally, we consider the scenario where SV 25 fails. This represents the worst of the four cases because SV 25 was the highest in elevation during the flight test. When this satellite is removed, the HDOP is 5.51 and the VDOP is 4.79. The vertical and horizontal accuracy of the two clock-aided solutions are shown in Figures 8.27-8.28. The clock-aided solution using the carrier-assisted clock model is more accurate than the standard clock-aided solution, although the difference is more marked in the horizontal position error than in the vertical position error. Thus, even with poor geometry and only three satellites, clock aiding allows continued navigation during the three-minute approach with vertical accuracy of about ±2 m and horizontal accuracy of about 1 m.

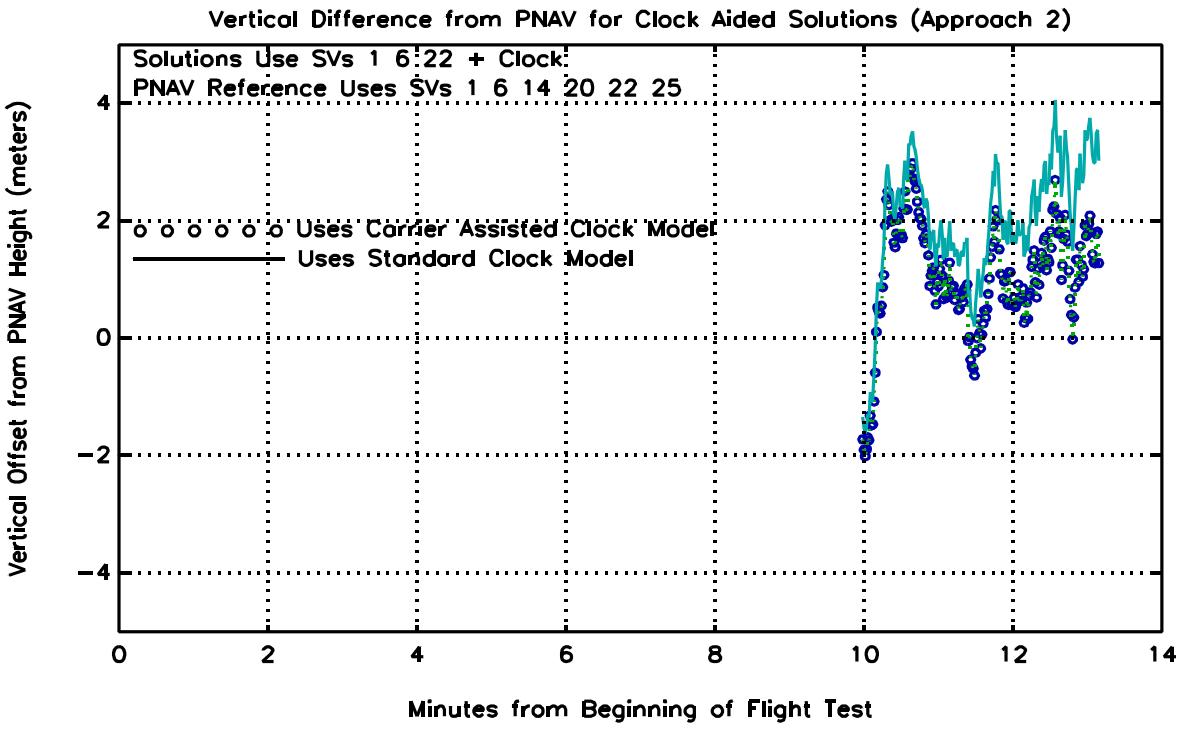

Figure 8.27 Vertical Offset from PNAV Solution for Clock Aided Solutions Using SVs 1 6 22 Plus Clock During Approach 2

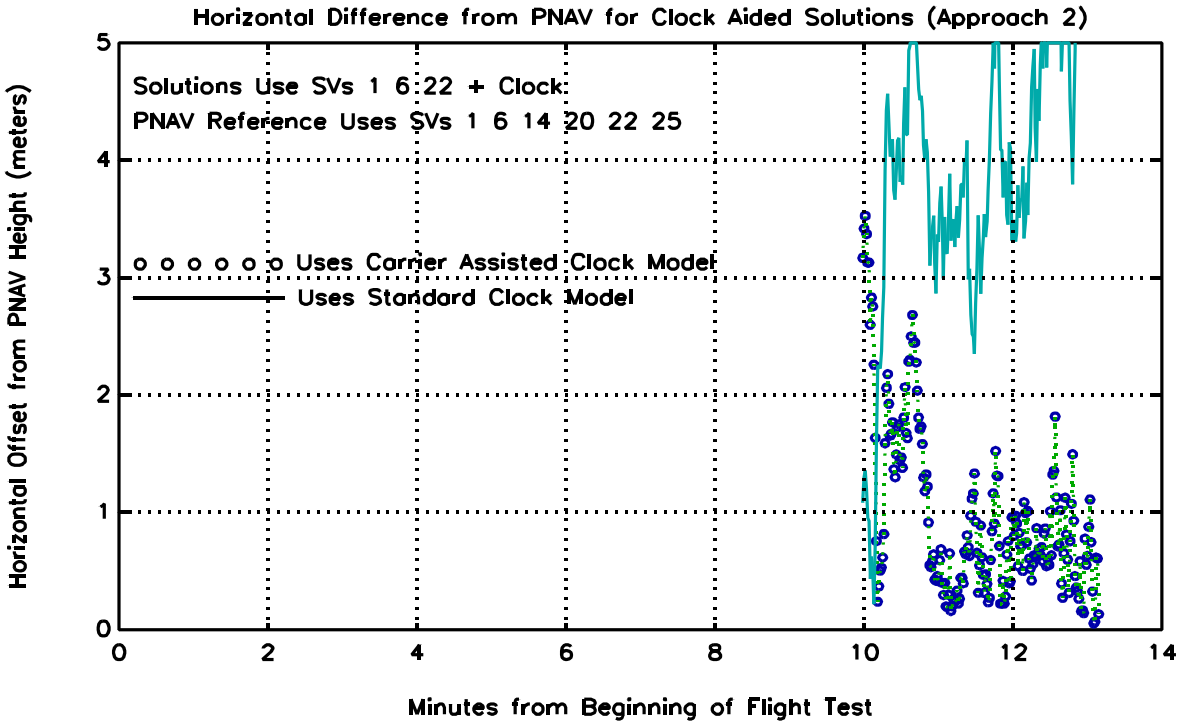

Figure 8.28 Horizontal Offset from PNAV Solution for Clock Aided Solutions Using SVs 1 6 22 Plus Clock During Approach 2

8.4 Conclusions from Flight Test of Clock-Aided Solutions

Because satellite failures can occur, it is possible that periods of high VDOP may be experienced as shown in Tables 8.1-8.2. The vertical accuracy for the clock-aided solutions is much better than unaided solutions using the same satellites. This shows that clock coasting should be used during periods of high VDOP to improve vertical accuracy. A clock model could also be used to improve vertical accuracy even when the geometry is good. Incorporating carrier phase measurements to improve the clock model provides better results than the standard clock model. Navigation with three satellites is possible if four satellites are available during a prior period so that a clock model can be formed. The carrier-assisted clock model does a better job of estimating the clock velocity and acceleration terms k_1 and k_2 than the standard clock model, and therefore achieves a better estimate of k_0 as well. The standard clock model also takes longer to converge on accurate coefficients than the carrier-assisted model. During periods of high VDOP it would be desirable to accurately model $c\Delta t_B$ in a short time, especially for an aircraft soon to initiate a final approach and landing. Misra (1995) has proposed using the previous 30 minutes of data to form a clock model. This may not always be practical, which means carrier phase measurements should be used to speed up the establishment of an accurate clock model.

Although the FAA would not allow a blind landing with three satellites plus a clock due to a lack of integrity monitoring, perhaps a nonprecision approach under conditions of good visibility would be allowed. In any case, carrier phase measurements should be used to optimize the clock model for the best performance.